

Supporting Information

Using highly emissive and environmentally sensitive *o*- carborane-functionalized metallophosphors to monitor mitochondrial polarity

Xiang Li,^[a] Xiao Tong,^[b] Yongheng Yin,^[a] Hong Yan,^{*[a]} Changsheng Lu^{*[a]}, Wei Huang^[b],
and Qiang Zhao^{*[b]}

^a State Key Laboratory of Coordination Chemistry, School of Chemistry and Chemical Engineering, Nanjing University, Nanjing, Jiangsu 210023, China.

^b Key Laboratory for Organic Electronics and Information Displays & Institute of Advanced Materials, National Jiangsu Synergetic Innovation Center for Advanced Materials, Nanjing University of Posts and Telecommunications, Nanjing, Jiangsu 210023, China.

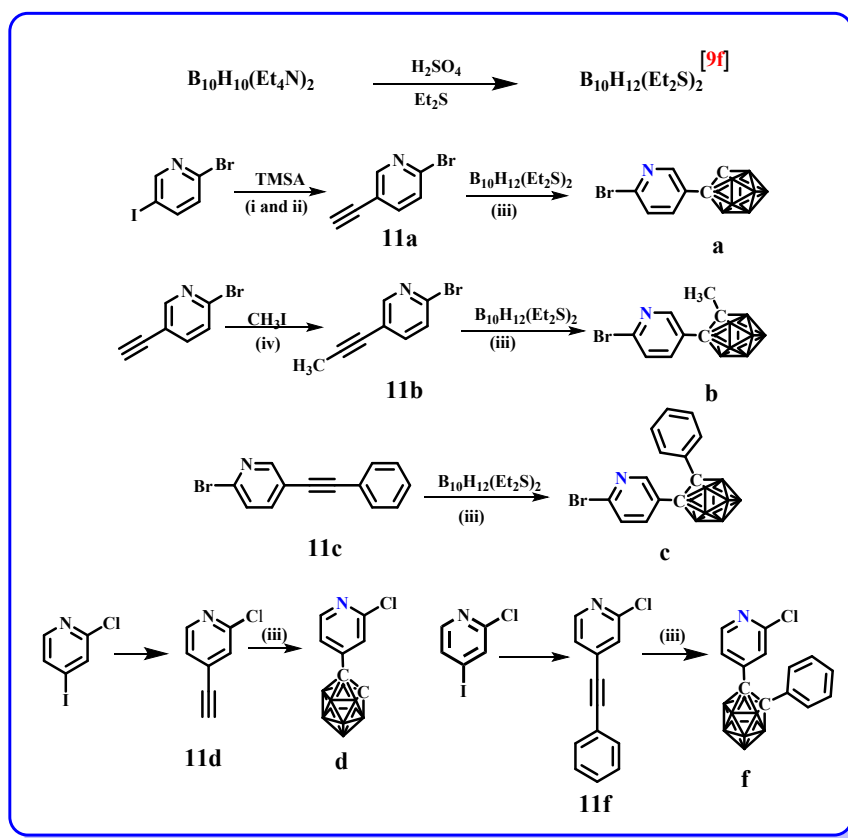
CONTENTS

- I. General method
- II. Synthesis
- III. X-ray structure determination
- IV. Quantum yields determination
- V. Quantum chemical calculations
- VI. Cytotoxicity test
- VII. Confocal luminescence imaging and phosphorescence lifetime imaging
- VII. References

I. General methods

In this paper, all the synthetic steps were carried out under an inert argon atmosphere using standard Schlenk and glovebox techniques unless otherwise noted. Commercial reagents were used without any further purification. All the solvents are freshly distilled, for example, THF and toluene were distilled on sodium / benzophenone as well as acetonitrile and EtOH on CaH₂. Dimeric [(C[^]N)₂Ir(μ-Cl)]₂ complex was prepared by literature procedures.^[S1] Intermediate compound B₁₀H₁₂(Et₂S)₂ was synthesized by a modified method according to literature reports.^[S2,S3a] Compounds **a**,^[S3a] **b**,^[S3a] **11c**,^[S3b] **11d**,^[S3c] and **11f**^[S3b] were synthesized according to literature. All NMR spectra (¹H-, ¹³C-, and ¹¹B-) were obtained at ambient temperature on Bruker DRX-400 or Bruker DRX-500 spectrometer. Chemical shifts are reported relative to CHCl₃ / CDCl₃ (δ ¹H = 7.26 ppm, δ ¹³C = 77.0 ppm) and external Et₂O·BF₃ (δ ¹¹B = 0 ppm), respectively. Mass spectra were measured with a Bruker Daltonics Autoflex IITM MALDI-TOF MS spectrometer, Micromass GC-TOF for EI-MS (70 eV) and a ESI-MS (LCQ Fleet, Thermo Fisher Scientific). Phosphorescence measurements were carried out by using a Hitachi F-4600 fluorescence spectrophotometer. Electronic absorption spectra were recorded with Shimadzu UV-2550 spectrophotometers. Melting points were measured with X4 digital melting point displayer. Phosphorescence lifetimes were determined by an Edinburgh instrument laser impulse fluorometer with picosecond time resolution. Elemental analyses for C, H and N were performed on a Vario MICRO elemental analyzer. IR data were collected on a Bruker Vacuum FT-IR Spectrometer 80 V. X-ray diffraction data were collected on a Bruker Smart CCD Apex DUO diffractometer with graphite monochromated Mo K α radiation ($\lambda = 0.71073 \text{ \AA}$) using the ω -2 θ scan mode.

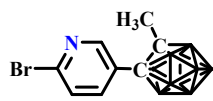
II: Synthesis



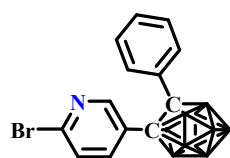
Scheme S1. Conditions: (i) TMSA, Pd(PPh₃)₂Cl₂, TEA / toluene. (ii) MeOH, K₂CO₃, r.t., overnight. (iii) B₁₀H₁₂(Et₂S)₂, toluene, 110 °C, refluxing for 3 days, MeOH. (iv) THF, MeI, LDA: lithiumdiisopropylamide, 2 h.

BrC1=CC=C(C#C)N=C1C2B10H12 **a**: To a toluene solution (80 mL) of **11a** (1.27 g, 7 mmol), B₁₀H₁₂(Et₂S)₂ (2.72 g, 9.1 mmol) was added at room temperature. The resulting reaction mixture was refluxed for three days. MeOH (50 mL) was then added to quench the reaction. Excessive solvent was removed under vacuum, and the resulting red solid was filtered and dissolved in toluene. Then the toluene solution passed an alumina column. After removal of solvent, a white solid was afforded. The crude product was purified by column chromatography using PE / DCM (V / V = 1:1) as eluent and afford **a** as a white solid (1.51 g, 72%). ¹H-NMR (CDCl₃) δ (ppm): δ 8.50 (d, *J* = 2.7 Hz, 1H), 7.68 (dd, *J* = 2.7, 8.5 Hz, 1H), 7.50 (d, *J* = 8.5 Hz, 1H), 3.93 (s, 1H, carborane-CH), 3.25–1.67 (br, 10H, B-H). ¹³C-NMR δ (ppm): 148.73, 144.04, 137.82, 129.15, 128.08, 72.67

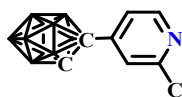
(B–C) and 60.23 (B–C). ^{11}B -NMR δ (ppm): -1.4 (1B), -3.4 (1B), -8.5 (2B), -10.9 (2B), -11.7 (2B), -12.4 (2B). $\text{C}_7\text{H}_{14}\text{B}_{10}\text{NBr}$. EI-MS (m/z): 300.20.



b: A procedure analogous to that for **a** was employed with **11b** (1.372 g, 7 mmol) and $\text{B}_{10}\text{H}_{12}(\text{Et}_2\text{S})_2$ (2.72 g, 9.1 mmol) to afford **b** as a white solid (1.50 g, 68%). ^1H -NMR (CDCl_3) δ (ppm): δ 8.63 (d, $J = 2.7$ Hz, 1H), 7.78 (dd, $J = 2.7, 8.5$ Hz, 1H), 7.55 (d, $J = 8.5$ Hz, 1H), 3.32–1.68 (br, 10H, B–H). ^{13}C -NMR δ (ppm): 151.88, 144.87, 140.58, 128.20, 126.83, 77.36 (B–C), 76.99 (B–C) and 23.35 (CH_3 -C). ^{11}B -NMR δ (ppm): -2.2 (2B), -4.2 (2B), -9.6 (6B). $\text{C}_8\text{H}_{16}\text{B}_{10}\text{NBr}$. EI-MS (m/z): 314.20.

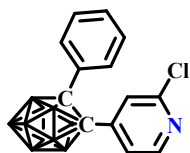


c: A procedure analogous to that for **a** was employed with **11c** (1.81 g, 7 mmol) and $\text{B}_{10}\text{H}_{12}(\text{Et}_2\text{S})_2$ (2.72 g, 9.2 mmol) to afford **c** as a white solid (1.71 g, 65%). ^1H NMR (CDCl_3) δ (ppm): δ 8.40 (d, $J = 2.7\text{Hz}$, 1H), 7.51 (dd, $J = 2.7, 8.5$ Hz, 1H), 7.44 (d, $J = 7.5$ Hz, 1H), 7.15–7.35 (m, 5H), 3.20–1.70 (br, 10H, B–H). ^{13}C NMR δ (ppm): 151.28, 144.17, 139.79, 130.81, 130.55, 129.76, 128.77, 127.43, 126.50, 85.11 (B–C) and 80.66 (B–C). ^{11}B NMR δ (ppm): 1.7 (2B), 1.0 (2B), -5.9 (2B), -6.7 (2B), -8.5 (2B). $\text{C}_8\text{H}_{16}\text{B}_{10}\text{NBr}$. EI-MS (m/z): 375.10.



d: To a toluene solution (80 mL) of **11d** (0.55 g, 4 mmol), the $\text{B}_{10}\text{H}_{12}(\text{Et}_2\text{S})_2$ (1.55 g, 5.2 mmol) was added at the room temperature. After heating to reflux, the reaction mixture was further stirred for three days. After the reaction finished, the MeOH (50 mL) was added to quench the reaction. The solvent was removed under vacuum, and the resulting red solid was filtered and dissolved in toluene. The solution was filtered on alumina column, and the solvent was removed in vacuum, affording a white solid. The crude compound was purified by column chromatography using PE / DCM (V / V = 1:1) as eluent, yielding pale-yellow solid 0.71 g (70%). ^1H NMR (CDCl_3): δ 8.40 (d, $J = 4.9$ Hz, 1H), 7.39 (s, 1H), 7.29 (d, $J = 4.9$ Hz, 1H), 3.98 (s, 1H, carborane-CH), 3.40–1.80 (br, 10H, B–H). ^{13}C NMR

(CDCl₃): δ (ppm) 152.55, 150.28, 144.86, 122.50, 120.54 (py-C), 72.50 (B-C) and 58.93 (B-C). ¹¹B NMR δ (ppm): 1.4 (2B), 0.1 (2B), -5.3 (2B), -8.1 (2B) and -9.5 (2B). EI-MS (m/z): 254.10.



f: A procedure analogous to that for **d** was employed with **If** (1.07 g, 5 mmol) and B₁₀H₁₂(Et₂S)₂ (1.94 g, 6.5 mmol) to afford **f** as a pale yellow solid (1.12 g, 68%). ¹H NMR (CDCl₃): δ 8.19 (d, J = 5.3 Hz, 1H), 7.45 (d, J = 7.4 Hz, 2H), 7.32 (d, J = 1.7 Hz, 2H), 7.19 (m, 3H), 3.50–1.70 (br, 10H, B-H). ¹¹B NMR (CDCl₃): δ 2.1 (1B), 0.8 (1B), -5.9 (2B), -6.7 (4B) and -8.6 (2B). EI-MS (m/z): 331.10.

III. X-ray structure determination

X-ray diffraction data were collected on a Bruker Smart CCD Apex DUO diffractometer with graphite monochromated Mo K α radiation (λ = 0.71073 Å) using the ω -2 θ scan mode. The data were corrected for Lorenz and polarization effects. Crystal structures were solved by direct methods and refined on F^2 by full-matrix least-squares methods using SHELXTL-2000. All calculations and molecular graphics were carried out using the SHELX-2000 program package and Mercury. CCDC 1496512 (**1f**), 1496513 (**2a**), 1496514 (**2b**), 1496515 (**2d**), 1496516 (**3b**), 1496517 (**3c**), 1496518 (**3e**), 1496519 (**4a**) and 1496520 (**Model**) contain the supplementary crystallographic data for this paper. These data can be obtained free of charge from the Cambridge Crystallographic Data Centre via www.ccdc.cam.ac.uk/conts/retrieving.html (or from the Cambridge Crystallographic Data Centre, 12, Union Road, Cambridge CB21EZ, UK; fax: (+44) 1223-336-033; or deposit@ccdc.cam.ac.uk).

Table S1. Crystallographic Data for **1f**, **2a**, **2b**, **2d**, **3b**, **3c**, **3e**, **4a**, and **Model**.

Compound	1f	2a	2b	2d
chemical formula	C ₁₈ H ₂₂ B ₁₀ N ₂	C ₃₄ H ₃₀ B ₁₀ N ₄ F ₄ IrPF ₆	C ₃₅ H ₃₂ B ₁₀ F ₄ N ₄ IrPF ₆	C ₃₇ H ₃₆ B ₁₀ F ₄ N ₄ IrPF ₆ ·2(CH ₂ Cl ₂)
formula weight	374.48	1015.91	1029.94	2575.06
crystal size (mm)	0.33 × 0.27 × 0.26	0.25 × 0.24 × 0.19	0.25 × 0.23 × 0.19	0.16 × 0.14 × 0.11
temperature (K)	291(2)	291(2)	291(2)	291(2)
radiation	0.71073	0.71073	0.71073	0.71073
crystal system	Orthorhombic	Monoclinic	Monoclinic	Monoclinic
space group	Pbca	P2(1)/c	P2(1)/c	C2/c
<i>a</i> (Å)	12.0727(15)	19.439(4)	19.3966(13)	41.094(3)
<i>b</i> (Å)	12.5640(16)	11.727(3)	11.8557(8)	11.9824(8)
<i>c</i> (Å)	26.304(3)	19.346(4)	19.0311(13)	19.1819(12)
<i>α</i> (°)	90	90	90	90
<i>β</i> (°)	90	100.293(4)	99.6930(10)	108.1890(10)
<i>γ</i> (°)	90.00	90	90	90
<i>V</i> (Å ³)	3989.8(9)	4339.3(17)	4313.9(5)	8973.3(10)
<i>Z</i>	8	4	4	8
<i>ρ</i> (calc) (g/cm ³)	1.247	1.553	1.586	1.692
<i>F</i> (000)	1552	1972	2008	4480
absorp. coeff. (mm ⁻¹)	0.065	3.187	3.207	3.208
<i>θ</i> range (deg)	1.55–27.51	1.06–25.01	2.02–25.01	1.04–27.54
reflns collected	33932	23133	30961	10315
indep. reflns	4571	7634	7562	10300

Refns obs. [$I > 2\sigma(I)$]	3755	6113	7058	8200
GOF	1.045	1.054	1.091	1.035
R1/wR2 [$I > 2\sigma(I)$]	0.0513/0.1363	0.0323/0.0893	0.0312/0.0821	0.0571/0.1418
R1/wR2 (all data)	0.0627/0.1473	0.0432/0.0935	0.0332/0.0840	0.0769/0.1566
Compound	3b	Model	3c	3e
chemical formula	$C_{35}H_{32}B_{10}F_4N_4IrPF_6 \cdot (CH_2Cl_2)$	$C_{32}H_{20}N_4F_4IrPF_6 \cdot C(H_2Cl_2) \cdot (Et_2O)$	$C_{40}H_{34}B_{10}F_4N_4IrPF_6$	$C_{38}H_{38}B_{10}F_4N_4IrPF_6 \cdot (CH_2Cl_2)$
formula weight	1114.87	1032.76	1092.00	1072.02
crystal size (mm)	$0.14 \times 0.13 \times 0.11$	$0.18 \times 0.16 \times 0.15$	$0.32 \times 0.27 \times 0.23$	$0.28 \times 0.22 \times 0.17$
temperature (K)	291(2)	123(2)	173(2)	173(2)
radiation	0.71073	0.71073	0.71073	0.71073
crystal system	Monoclinic	Orthorhombic	Triclinic	Monoclinic
space group	P2(1)/c	P2(1)2(1)2(1)	P-1	P2(1)/n
$a(\text{\AA})$	17.3958(14)	9.6791(14)	10.4515(4)	10.3413(5)
$b(\text{\AA})$	12.1322(10)	12.7772(18)	13.4143(6)	19.9619(9)
$c(\text{\AA})$	24.263(2)	28.988(4)	18.7342(8)	23.7940(11)
$\alpha(^{\circ})$	90	90	96.628(2)	90.00
$\beta(^{\circ})$	106.7550(10)	90	97.7990(10)	94.8920(10)
$\gamma(^{\circ})$	90.00	90	105.8630(10)	90.00
$V(\text{\AA}^3)$	4903.3(7)	3585.0(9)	2470.87(18)	4894.0(4)
Z	4	4	2	4
$\rho(\text{calc})$ (g/cm ³)	1.510	1.845	1.468	1.685
F (000)	2176	1940	1068	2440
absorp.coeff.	2.934	4.005	2.805	3.054

(mm ⁻¹)				
θ range (deg)	1.22–25.50	1.40–27.63	3.06–25.40	3.02–25.24
reflns collected	20948	32482	24331	28090
indep. reflns	8866	8309	8977	8918
Refns obs. [$I > 2\sigma(I)$]	7363	8158	7750	6344
GOF	1.071	1.129	1.026	1.020
R1/wR2 [$I > 2\sigma(I)$]	0.0347/0.0950	0.0236/0.0579	0.0386/0.0460	0.0788/0.0877
R1/wR2 (all data)	0.0437/0.0992	0.0246/0.0618	0.0400/0.0299	0.0419/0.0776
Compound	4a			
chemical formula	C ₁₄ H ₂₈ B ₂₀ N ₂			
formula weight	440.2			
crystal size (mm)	0.25 × 0.14 × 0.12			
temperature (K)	291(2)			
radiation	0.71073			
crystal system	Monoclinic			
space group	C2/c			
<i>a</i> (Å)	30.853(15)			
<i>b</i> (Å)	6.836(3)			
<i>c</i> (Å)	12.622(6)			
<i>α</i> (°)	90			
<i>β</i> (°)	106.229(9)			

$\gamma(^{\circ})$	90.00
V(\AA^3)	2556(2)
Z	4
$\rho(\text{calc})$ (g/cm ³)	1.229
F (000)	950
absorp.coeff. (mm ⁻¹)	0.075
θ range (deg)	1.37–28.61
reflns collected	8648
indep. reflns	3123
Refns obs. [$I >$ $2\sigma(I)$]	1320
GOF	1.046
R1/wR2 [$I >$ $2\sigma(I)$]	0.1072/0.3291
R1/wR2 [all data]	0.1757/0.2855

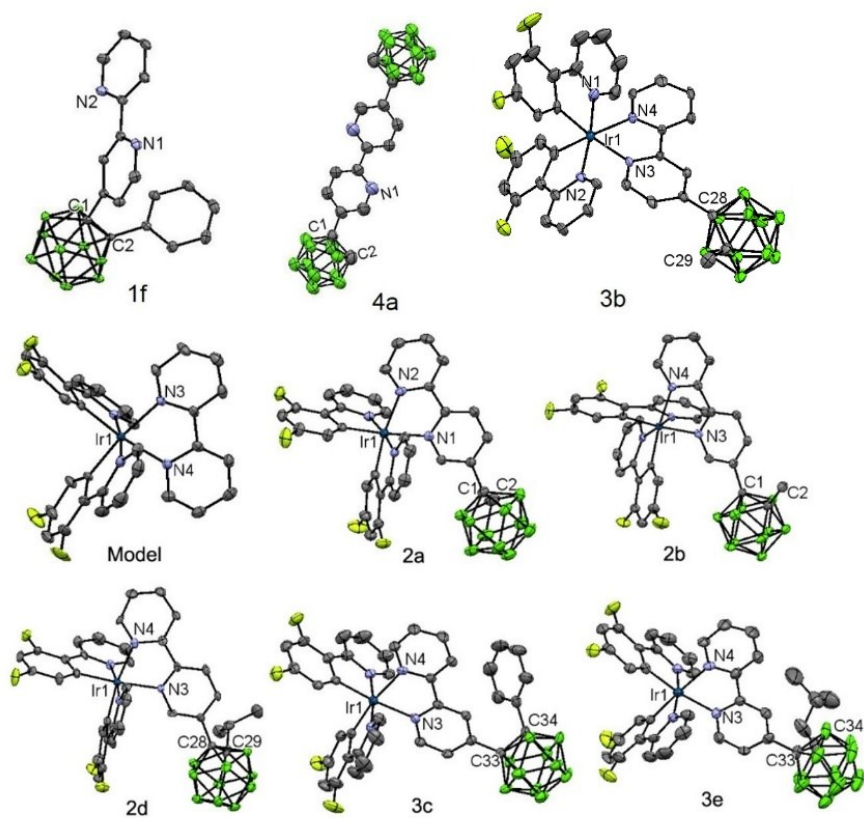


Figure S1. ORTEP diagrams of ligands **1f**, **4a**, and complexes **Model**, **2a**, **2b**, **2d**, **3b**, **3c**, and **3e** with thermal ellipsoids drawn at the 30% probability level. H atoms are omitted for clarity.

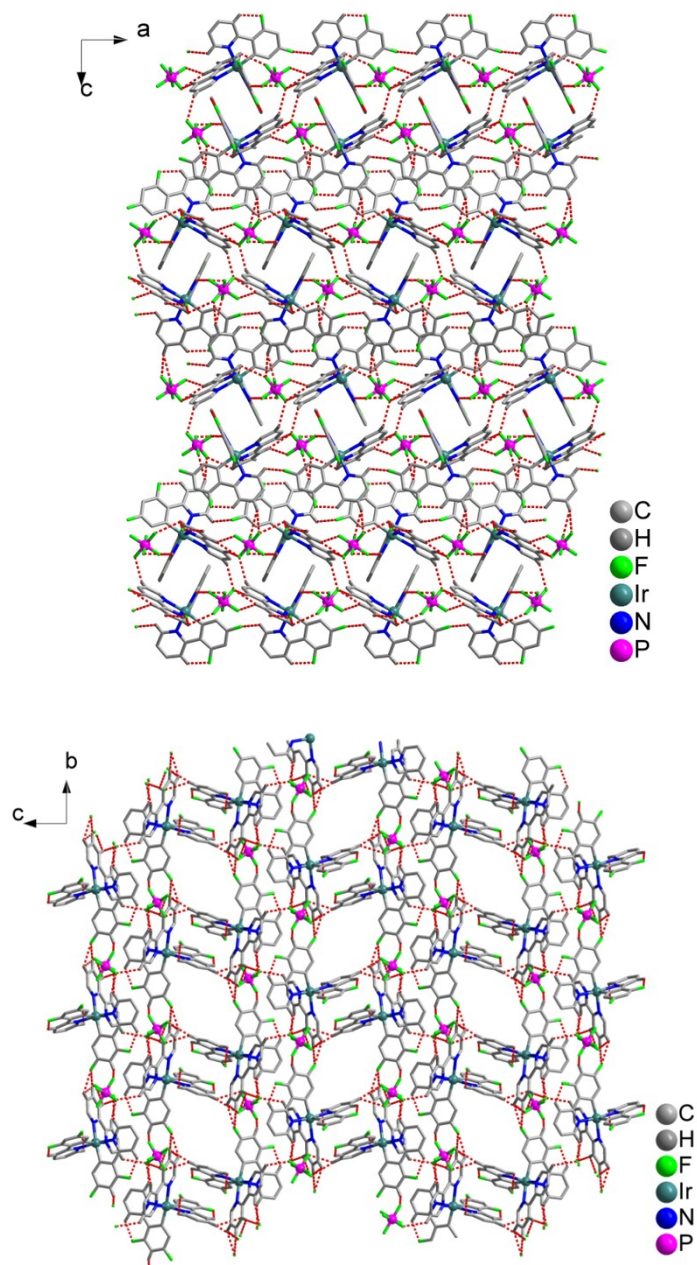


Figure S2. The intermolecular packing of **Model** in solid state (in crystals). (red lines show the H bonding).

Note: Although complex **Model** (CCDC: 1496520) has been reported, but there is no crystal structure data. Complex **model** was packed in an orthorhombic crystal structure with space group $P2(1)2(1)2(1)$ (Figures 1 and S1). As depicted in Figure S2, the complex **model** is closely packed and there are a lot of H-bonds between the different molecular layers. Because of the F atoms from both phenyl ring and PF_6 , the interactions generated by the hydrogen bonds are very strong, which might be the reason why the model complex is badly quenched in solid state.

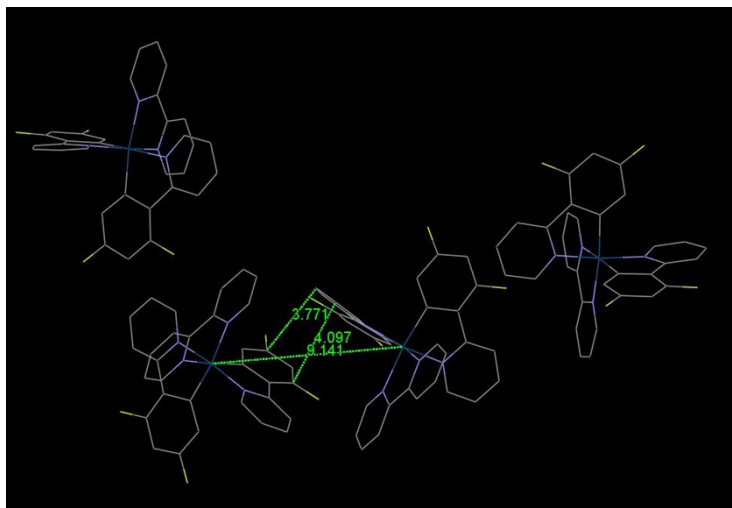


Figure S3. The intermolecular packing of **model** in solid state (in crystals).

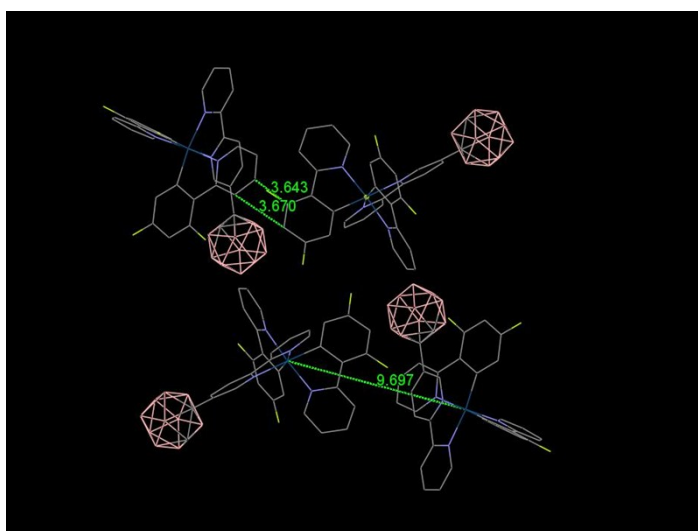


Figure S4. The intermolecular packing of **2a** in solid state (in crystals).

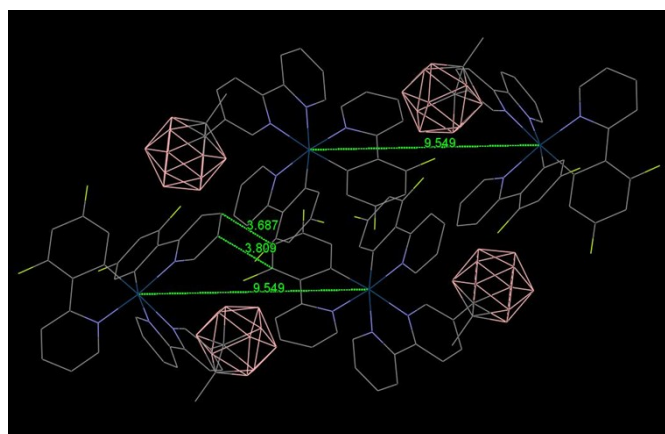


Figure S5. The intermolecular packing of **2b** in solid state (in crystals).

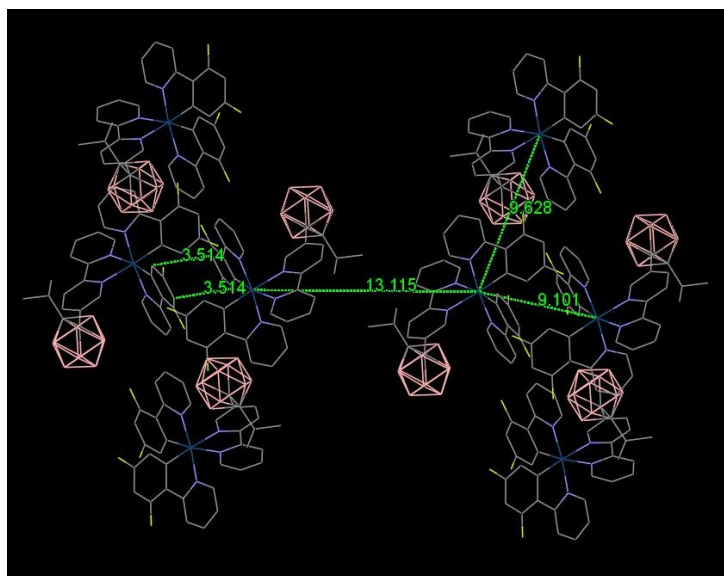


Figure S6. The intermolecular packing of **2d** in solid state (in crystals).

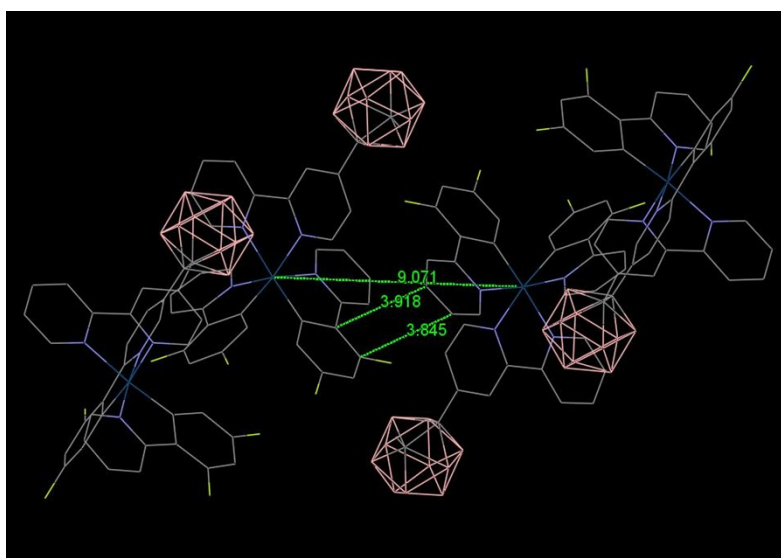


Figure S7. The intermolecular packing of **3b** in solid state (in crystals).

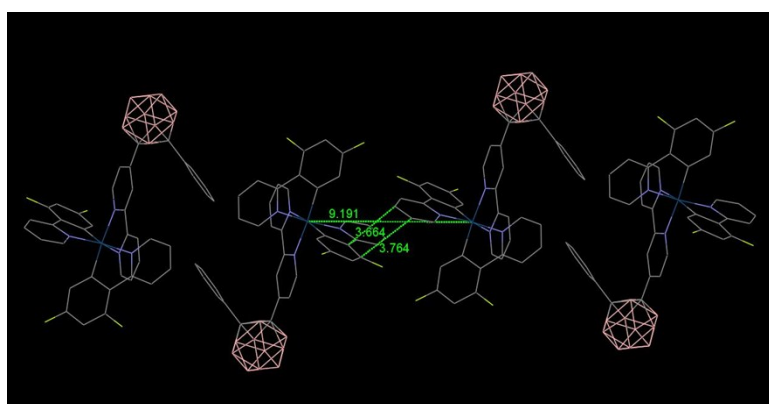


Figure S8. The intermolecular packing of **3c** in solid state (in crystals).

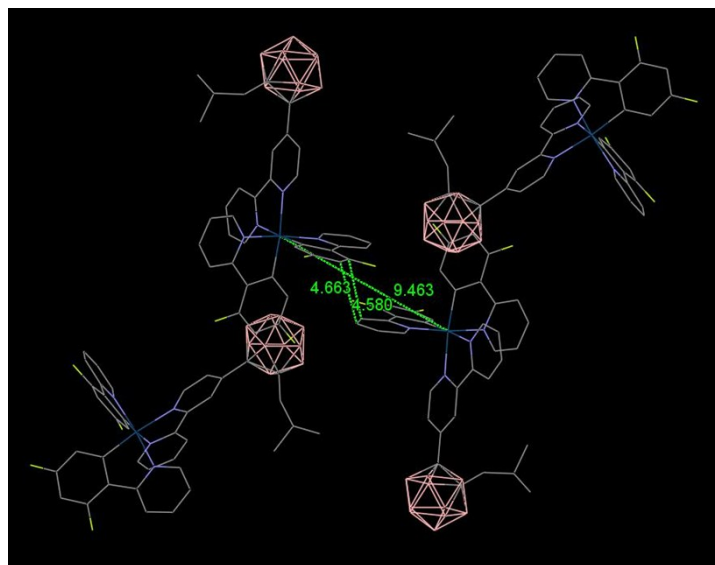


Figure S9. The intermolecular packing of **3e** in solid state (in crystals).

IV. Quantum yields determination

Absolute quantum yields of all the complexes in CH_2Cl_2 and in solid states were measured by employing an integrating sphere. Phosphorescence lifetime studies were performed with an Edinburgh FL 920 photo counting system with a hydrogen-filled lamp as the excitation source.

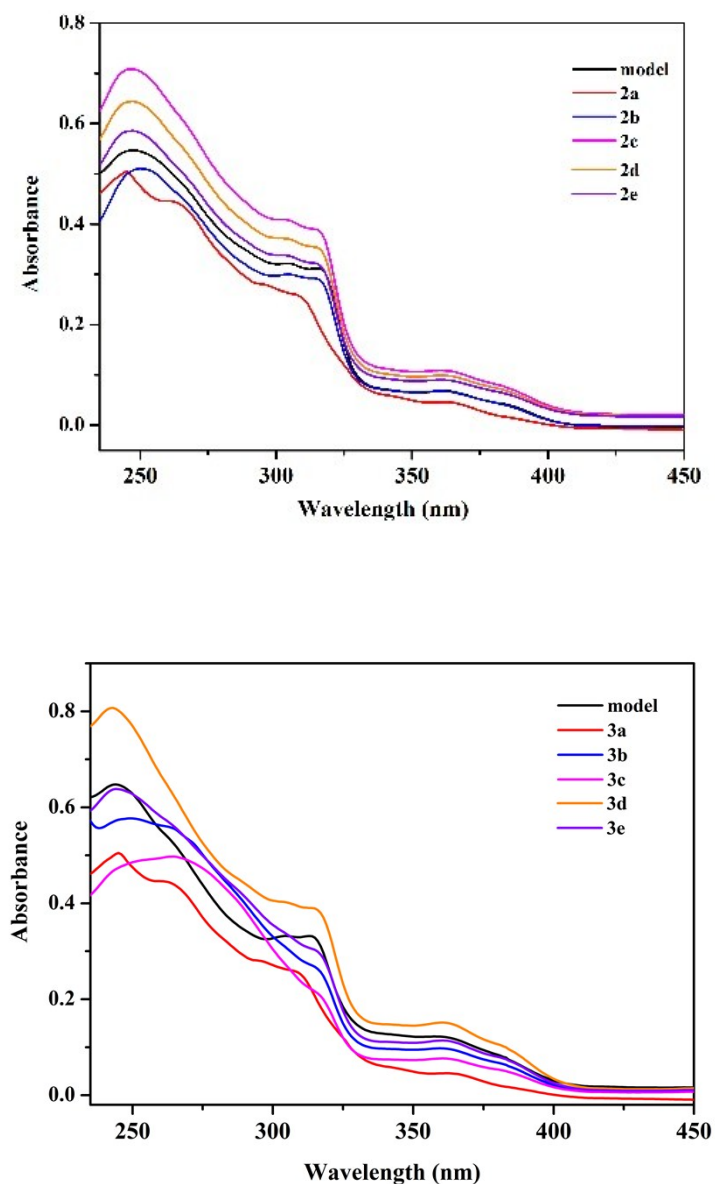


Figure S10. Absorption spectra: **Up)** complexes for **2a**, **2b**, **2c**, **2d**, **2e**, and **Model**; **Down)** complexes for **3a**, **3b**, **3c**, **3d**, **3e**, and **Model** in degassed CH_2Cl_2 at room temperature.

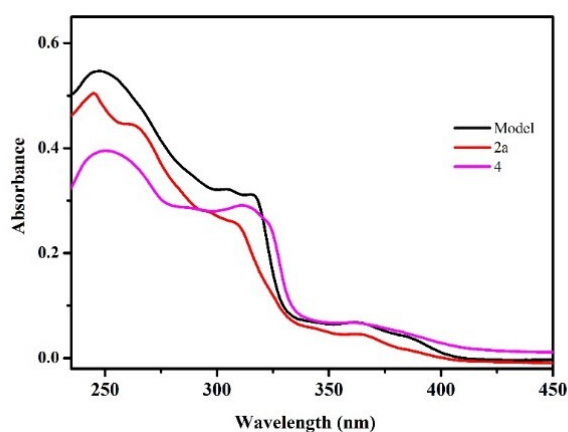


Figure S11. The compared absorption spectra of complexes for **2a**, **4**, and **Model** in degassed CH_2Cl_2 at room temperature.

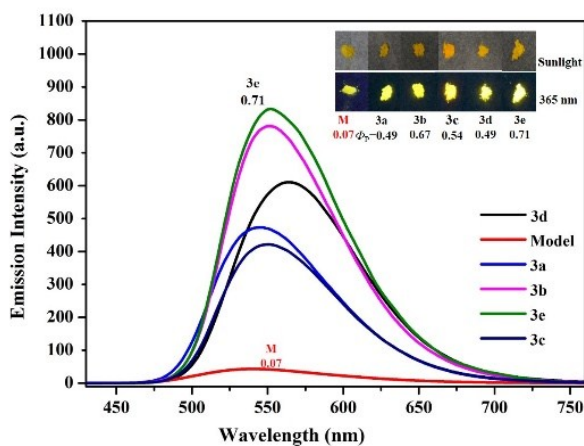
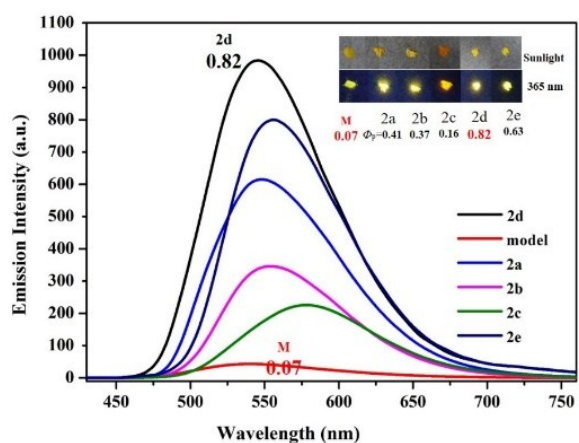
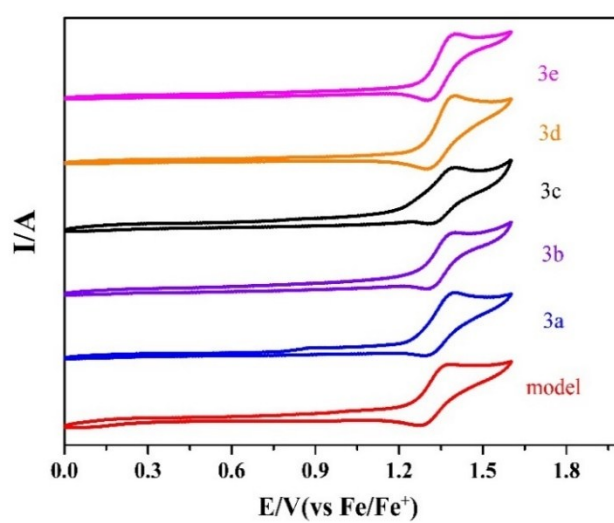
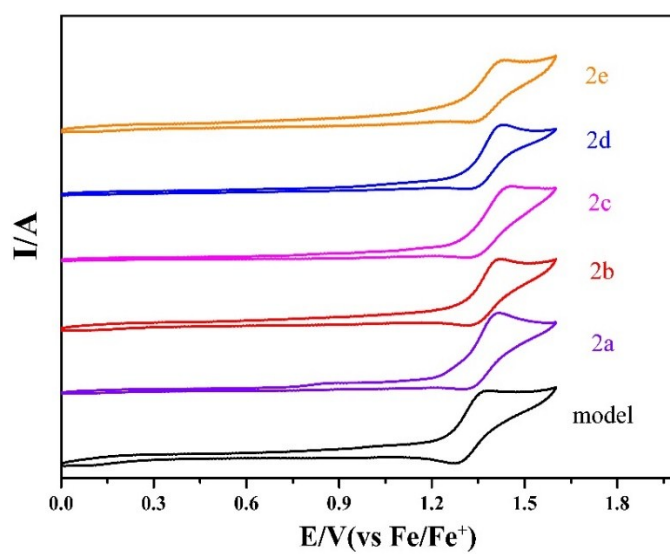


Figure S12. Solid state emission PL spectra of the iridium (III) complexes: **Up**) complexes for **2a**, **2b**, **2c**, **2d**, **2e**, and **Model**; **Down**) complexes for **3a**, **3b**, **3c**, **3d**, **3e**, and **Model** in solid states at room temperature under the same conditions. ($\lambda_{\text{ex}} = 365 \text{ nm}$ and corresponding luminescence photographs inseted).

Table S2. Calculated volume of the iridium(III) complexes.

Complexes	Model	2a	2b	2c	2d	2e	3a	3b	3c	3d	3e
V(cm ³ / mol)	408.4	449.9	453.3	500.2	523.3	580.9	479.6	497.7	560.5	497.0	461.4



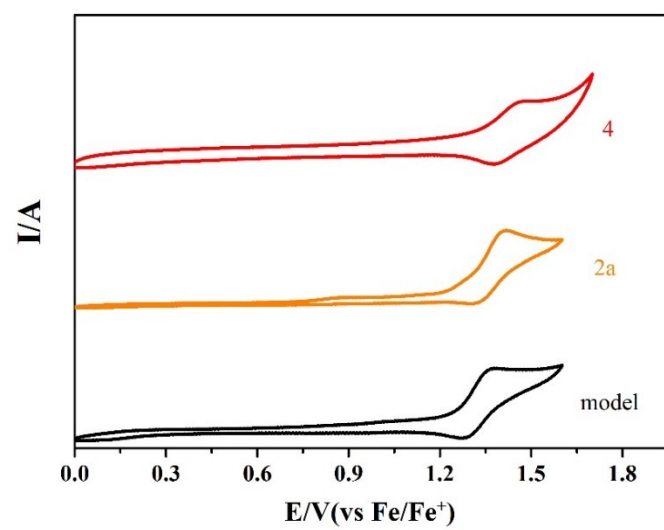


Figure S13. Cyclic voltammograms of iridium(III) complexes under a scan rate of 100 mV / s.

Table S3. Solution emission data of complexes in different degassed solvents at room temperature.

Complexes	Solvents	λ_{em} [nm]	Φ_{PL}	τ [ns]
Model	toluene	521	0.47	561.5
	CH ₂ Cl ₂	520	0.26	811.5
	CHCl ₃	519	0.38	461.8
	CH ₃ CN	529	0.34	397.7
	ethanol	521	0.33	325.1
	DMSO	530	0.19	286.8
	2a	toluene	544	0.62
CH ₂ Cl ₂		563	0.49	1115.0
CHCl ₃		542	0.70	1158.8
CH ₃ CN		564	0.35	651.0
ethanol		551	0.50	915.8
DMSO		563	0.17	631.5
2b		toluene	545	0.42
	CH ₂ Cl ₂	563	0.59	746.9
	CHCl ₃	553	0.45	1037.3
	CH ₃ CN	570	0.39	636.9
	ethanol	561	0.28	679.7
	DMSO	576	0.28	453.9
	2c	toluene	553	0.43
CH ₂ Cl ₂		560	0.62	794.0
CHCl ₃		546	0.71	1037.9
CH ₃ CN		526	0.40	1044.3
ethanol		539	0.25	900.8
DMSO		519	0.20	1257.5
2d		toluene	535	0.80
	CH ₂ Cl ₂	563	0.79	760.0
	CHCl ₃	553	0.72	581.5
	CH ₃ CN	574	0.40	385.5
	ethanol	567	0.34	324.1
	DMSO	577	0.21	185.2
	2e	toluene	545	0.49
CH ₂ Cl ₂		563	0.72	774.6
CHCl ₃		553	0.82	1032.4
CH ₃ CN		568	0.45	639.5
ethanol		561	0.52	722.8

Complexes	Solvents	λ_{em} [nm]	Φ_{PL}	τ [ns]
	DMSO	563	0.25	529.1
3a	toluene	528	0.57	887.3
	CH ₂ Cl ₂	555	0.55	585.3
	CHCl ₃	530	0.86	803.0
	CH ₃ CN	547	0.28	493.4
	ethanol	547	0.46	840.9
	DMSO	535	0.28	897.7
3b	toluene	542	0.73	785.5
	CH ₂ Cl ₂	555	0.66	733.0
	CHCl ₃	547	0.88	1017.4
	CH ₃ CN	558	0.34	544.7
	ethanol	559	0.59	901.3
	DMSO	536	0.12	939.3
3c	toluene	552	0.26	517.9
	CH ₂ Cl ₂	553	0.68	465.1
	CHCl ₃	550	0.10	547.2
	CH ₃ CN	525	0.03	753.1
	ethanol	556	0.07	114.4
	DMSO	528	0.04	900.4
3d	toluene	546	0.38	779.5
	CH ₂ Cl ₂	556	0.76	759.3
	CHCl ₃	552	0.43	1012.9
	CH ₃ CN	529	0.07	904.6
	ethanol	560	0.14	728.6
	DMSO	525	0.14	1017.1
3e	toluene	552	0.60	799.1
	CH ₂ Cl ₂	556	0.73	793.6
	CHCl ₃	552	0.09	1012.2
	CH ₃ CN	565	0.10	142.13
	ethanol	560	0.60	858.3
	DMSO	546	0.17	919.9
4	toluene	571	0.39	782.0
	CH ₂ Cl ₂	594	0.33	597.5
	CHCl ₃	572	0.32	536.5
	CH ₃ CN	597	0.27	270.0
	ethanol	590	0.26	258.9
	DMSO	598	0.13	198.1

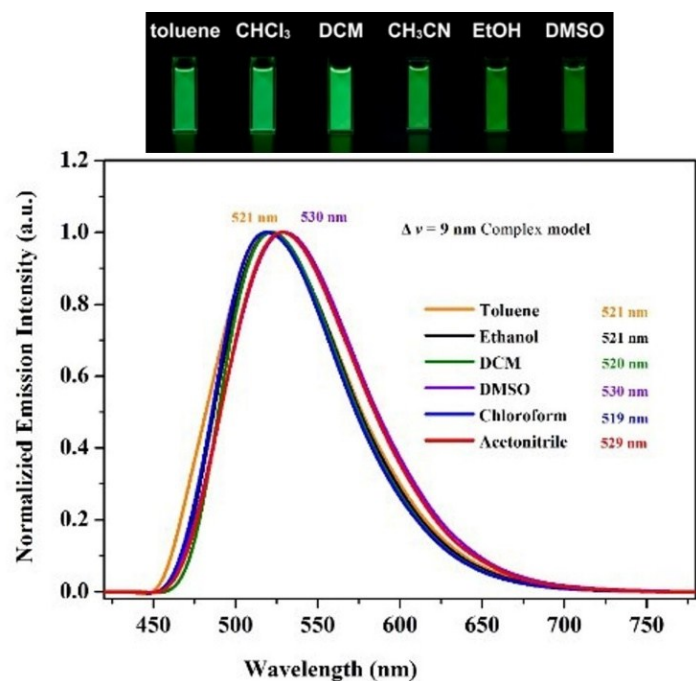
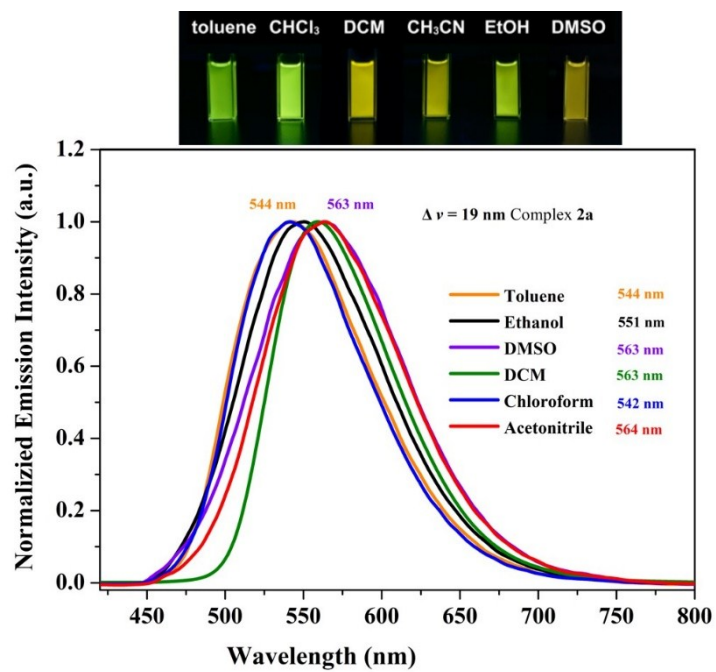


Figure S14. Solution emission PL spectra of complexes **Model** in different degassed solvents at room temperature. (Up: photos of the phosphorescence emission of **Model** in various solvents).



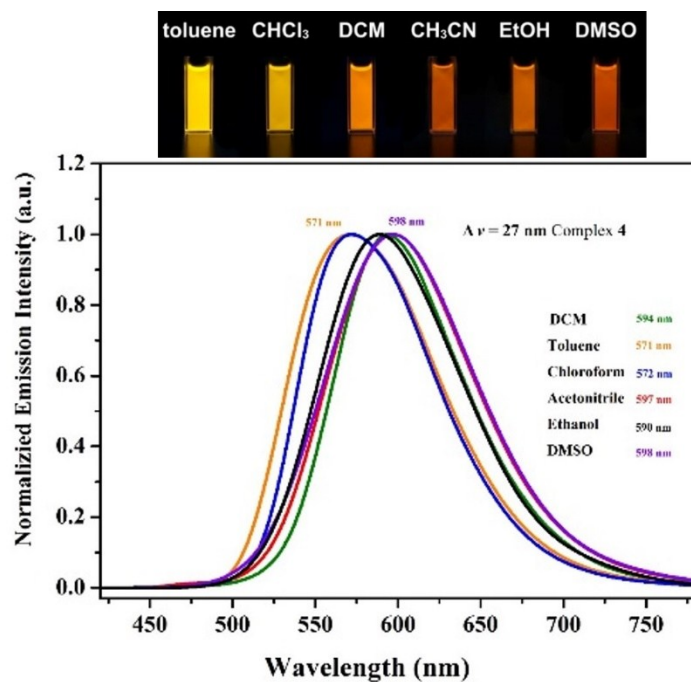
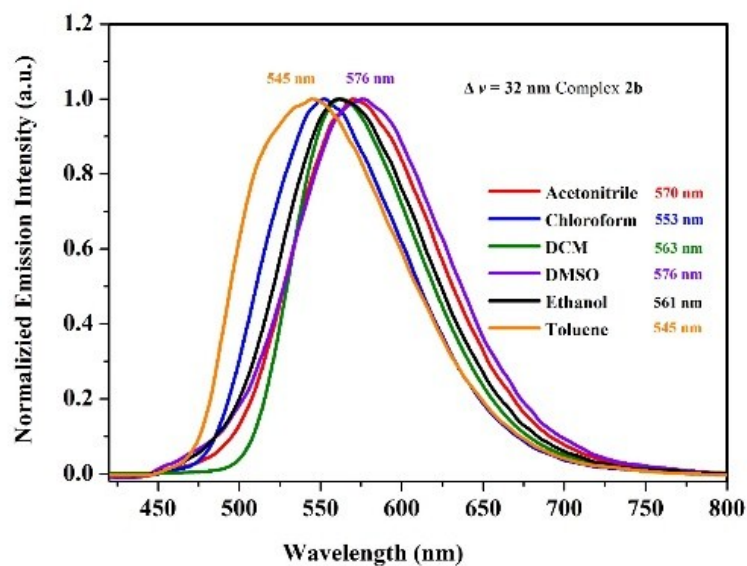


Figure S15. Solution emission PL spectra of complexes **2a** (up) and **4** (down) in different degassed solvents at room temperature. (Up: photos of the phosphorescence emission of **2a** and **4** in various solvents).



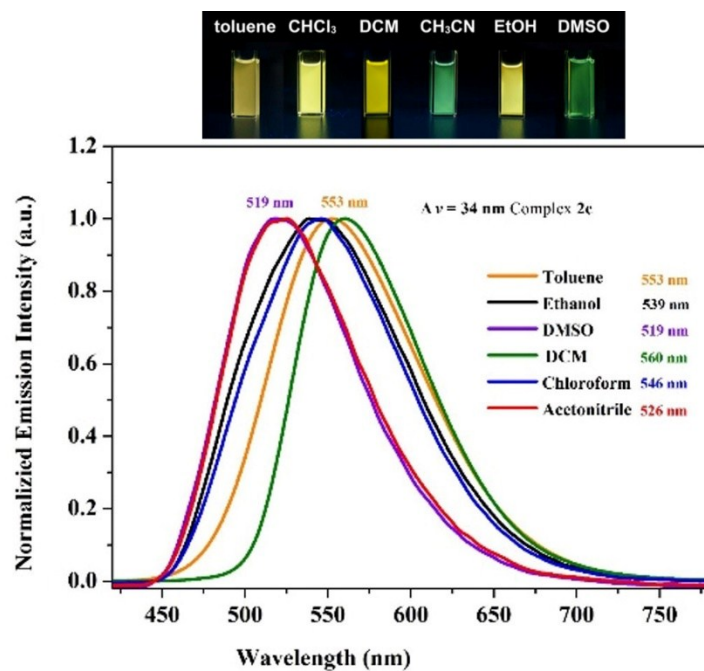
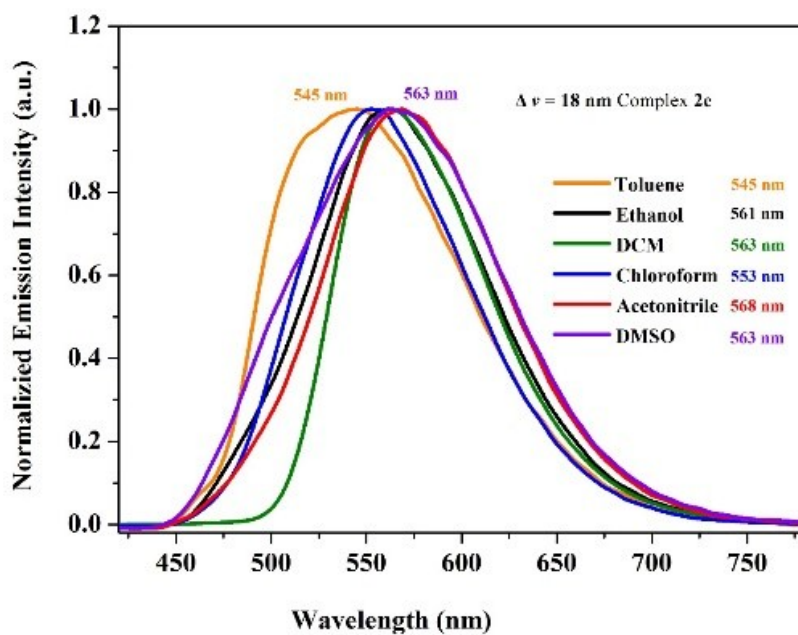


Figure S16. Solution emission PL spectra of complexes **2b** (up) and **2c** (down) in different degassed solvents at room temperature. (Up: photos of the phosphorescence emission of **2c** in various solvents).



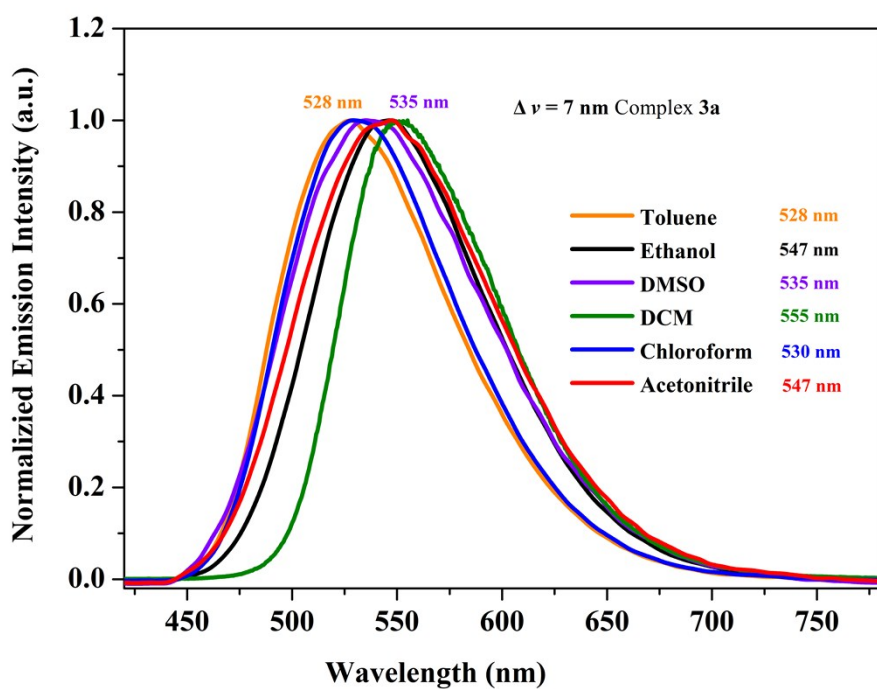
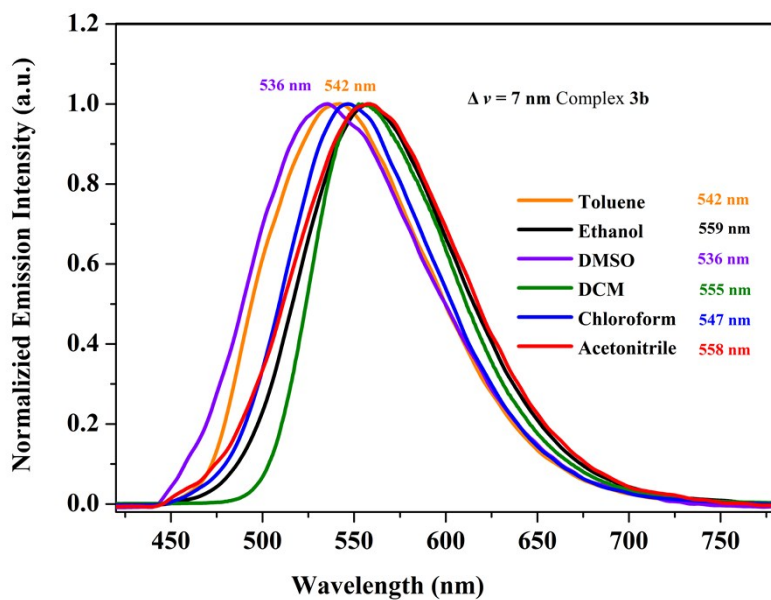


Figure S17. Solution emission PL spectra of complexes 2e (up) and 3a (down) in different degassed solvents at room temperature.



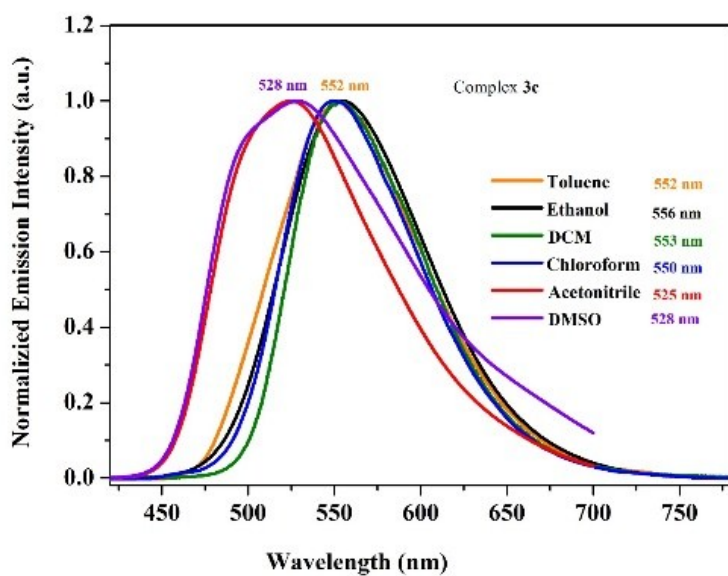
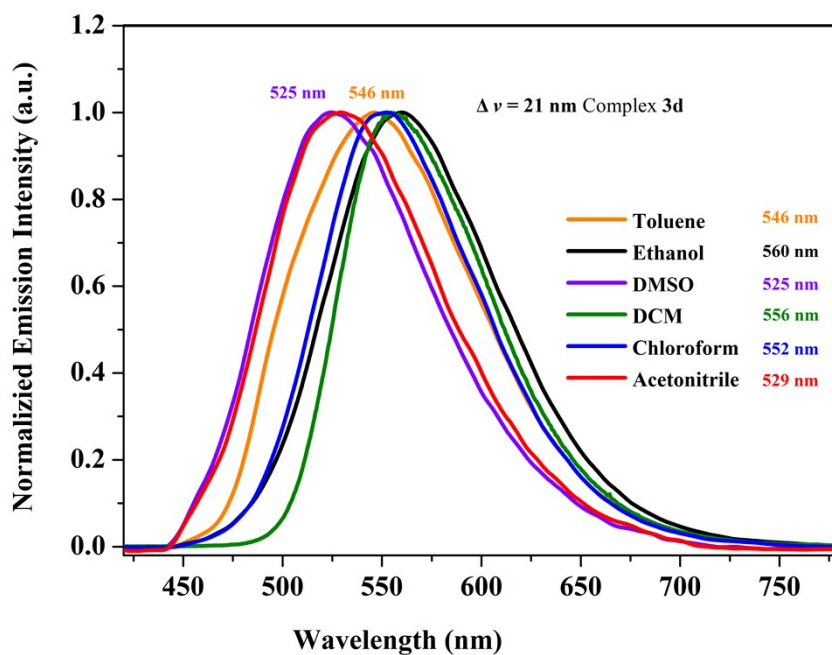


Figure S18. Solution emission PL spectra of complexes **3b** (up) and **3c** (down) in different degassed solvents at room temperature.



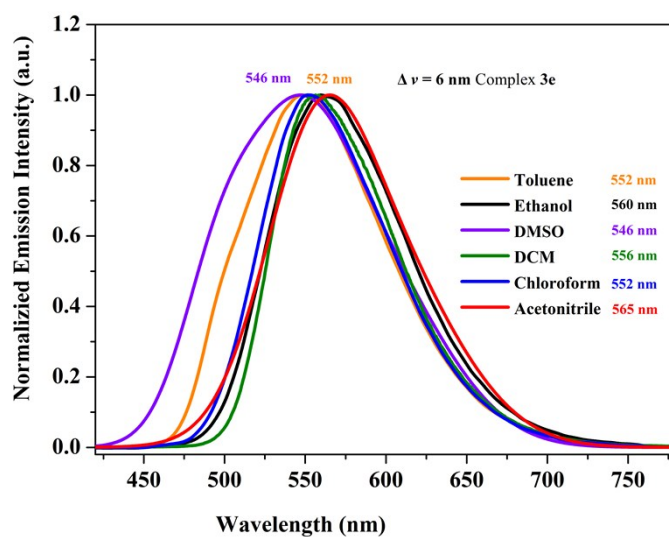


Figure S19. Solution emission PL spectra of complexes **3d** (up) and **3e** (down) in different degassed solvents at room temperature.

V. Quantum chemical calculations

Geometries of the iridium(III) complexes were optimized by the density functional theory (DFT) method based on obtained crystal structures. The electronic transition energies including electron correlation effects were computed by the time dependent density functional theory (TD-DFT) method using B3LYP functional (TD-B3LYP). The PCM method was used to treat the different solvents. LANL2DZ basis set was used to treat the heavy metal iridium atom, whilst M06 functional with a basis set of 6-31G (d,p) for C, H, N, F, and B atoms. All calculations described here were performed by the Gaussian 09 program. Frequency calculations were also carried out at the B3LYP / LANL2DZ/6-31G (d,p) level. All were found to be true minima based on no imaginary frequencies found.^[S4]

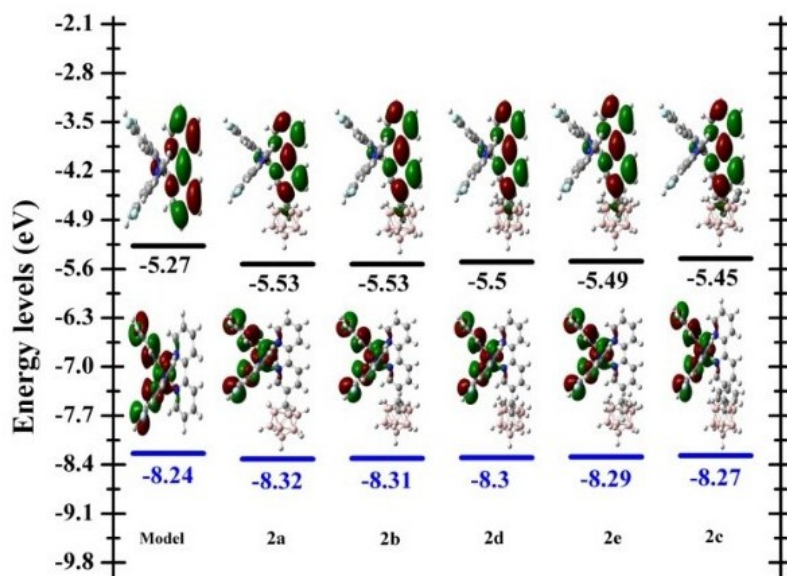


Figure S20. Calculated HOMO and LUMO of iridium(III) complexes in the ground state (S_0).

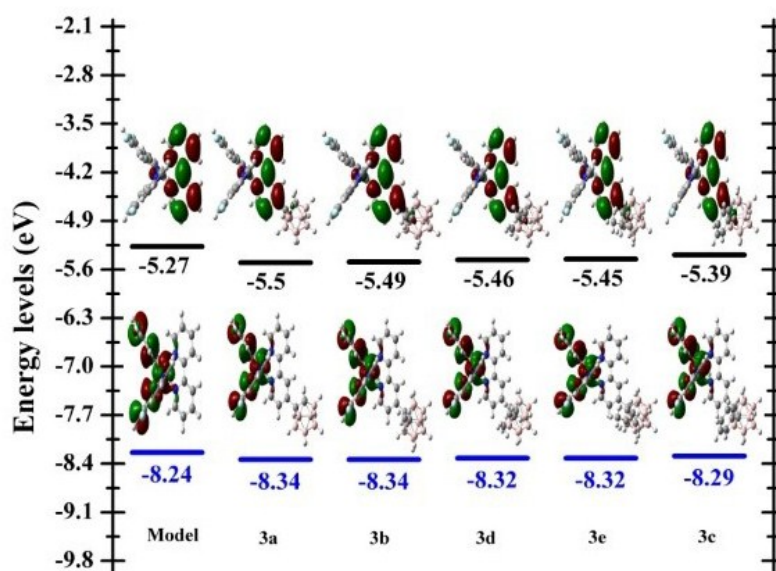
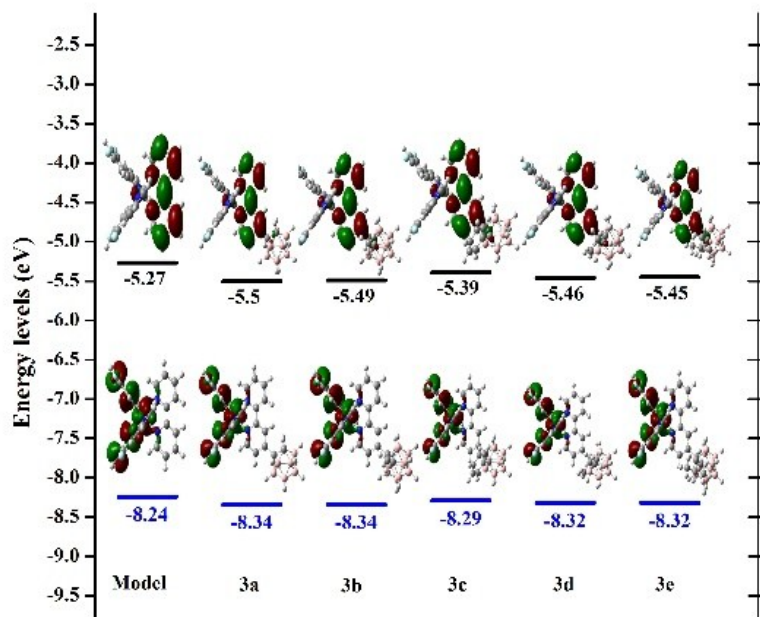
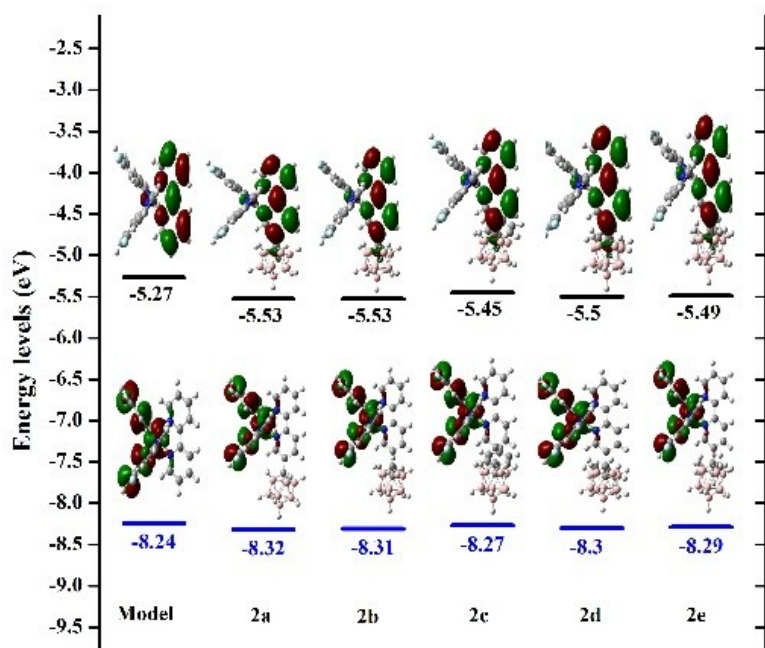


Figure S21. Calculated HOMO and LUMO of iridium(III) complexes in the ground state (S_0).



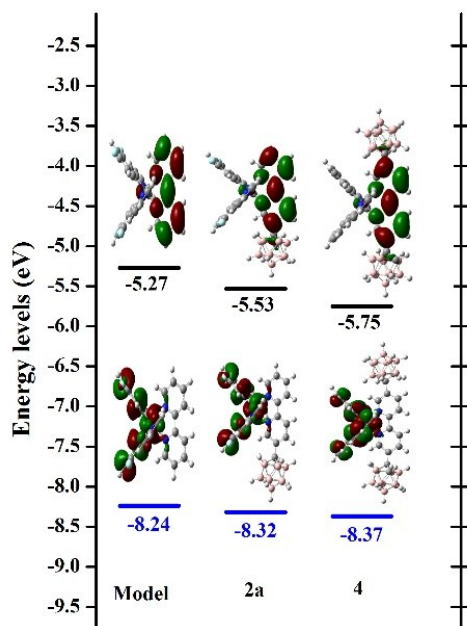


Figure S22. Calculated HOMO and LUMO at the excited state (T_1) for complexes. Blue (HOMO orbitals) and black (LUMO orbitals).

Table S4. Calculated dipole moments of iridium complexes in both ground state and excited state.

Compounds	Dipole moment (ground state) (D)	Dipole moment (excited state) (D)
Model	95.8668	87.4262
2a	39.1906	48.4686
2b	39.0265	48.3980
2c	38.8193	48.2520
2d	38.9707	48.4742
2e	38.4196	47.8520
3a	39.3903	49.7797
3b	39.2503	50.0461
3c	39.5400	49.8262
3d	39.4417	50.0961
3e	39.1137	49.2509
4	36.2498	43.4271

Table S5. Calculated dipole moments of iridium complexes in ground state (S_0) with different solvents.

Solvents	Toluene(D)	DCM	CHCl ₃	CH ₃ CN	EtOH	DMSO
Model	97.4198	98.8331	98.2954	99.3747	99.2894	99.4223
2a	39.0762	38.8261	38.9434	38.6640	38.6929	38.6474
2b	39.0069	38.8616	38.9162	38.7717	38.7879	38.7608
2c	38.8943	38.9434	38.9323	38.9250	38.9319	38.9197
2d	38.9536	38.8884	38.9252	38.8361	38.8448	38.8317
2e	38.3230	38.1960	38.2504	38.1463	38.1499	38.1477
3a	39.7102	39.7981	39.7910	39.7611	39.7702	39.7559
3b	39.6330	39.7773	39.7491	40.0160	40.0114	40.0087
3c	82.8126	82.6059	83.3347	82.5185	82.6431	82.5963
3d	39.9518	40.3535	40.2445	40.3802	40.4058	40.3916
3e	39.6921	40.0479	39.9334	40.1308	40.1200	40.1366
4	34.9124	33.3893	34.0136	32.7215	32.8284	32.6619

Table S6. Calculated dipole moments of iridium complexes in excited state (T_1) with different solvents.

Solvents	Toluene(D)	DCM	CHCl ₃	CH ₃ CN	EtOH	DMSO
Complexes						
Model	87.1334	86.9102	86.9984	86.8089	86.8259	86.7992
2a	49.8667	51.4706	50.6414	51.9313	51.8621	51.9715
2b	50.3696	52.0249	51.3873	52.7076	52.5976	53.2287
2c	50.3600	61.0891	57.5522	64.3914	64.2030	64.6781
2d	50.5032	52.3258	51.4612	61.0291	60.3769	61.8413
2e	49.5692	51.2514	50.5971	51.9666	51.8459	52.0361
3a	51.6776	53.1052	52.5900	53.5914	53.5172	53.6327
3b	52.2590	54.2348	53.4325	54.9360	54.8242	55.0004
3c	52.4100	69.3166	54.1923	72.0359	71.6483	72.2374
3d	52.4575	54.7352	53.8424	55.9346	55.6924	56.1177
3e	51.6176	53.8763	53.0270	54.8551	54.7111	54.9402
4	43.4848	43.4473	43.4441	44.5101	45.0966	44.5187

Table S7. Calculated transition dipole moments (ΔT_1-S_0) of iridium complexes in different solvents.

Solvents \ Complexes	Toluene(D)	DCM	CHCl ₃	CH ₃ CN	EtOH	DMSO
Model	-10.2864	-11.9229	-11.297	-12.5658	-12.4635	-12.6231
2a	10.7905	12.6445	11.698	13.2673	13.1692	13.3241
2b	11.3627	13.1633	12.4711	13.9359	13.8097	14.4679
2c	11.4657	22.1457	18.6199	25.4664	25.2711	25.7584
2d	11.5496	13.4374	12.536	22.193	21.5321	23.0096
2e	11.2462	13.0554	12.3467	13.8203	13.696	13.8884
3a	11.9674	13.3071	12.799	13.8303	13.747	13.8768
3b	12.626	14.4575	13.6834	14.92	14.8128	14.9917
3c	-30.4026	-13.2893	-29.1424	-10.4826	-10.9948	-10.3589
3d	12.5057	14.3817	13.5979	15.5544	15.2866	15.7261
3e	11.9255	13.8284	13.0936	14.7243	14.5911	14.8036
4	8.5724	10.058	9.4305	11.7886	12.2682	11.8568

VI. Cytotoxicity

pH Dependence. Because of the poor solubility of complex **2d** in water, the phosphorescence spectra of **2d** (1 μM) were measured in mixed solvents of DMSO and pH buffer (7:3 v/v). The following buffers were prepared; KCl / HCl for pH 1–2, citric acid/ Na_2HPO_4 for pH 3–6, Na_2HPO_4 / NaH_2PO_4 for pH 7–8 and Na_2CO_3 / NaHCO_3 for pH 9–11).

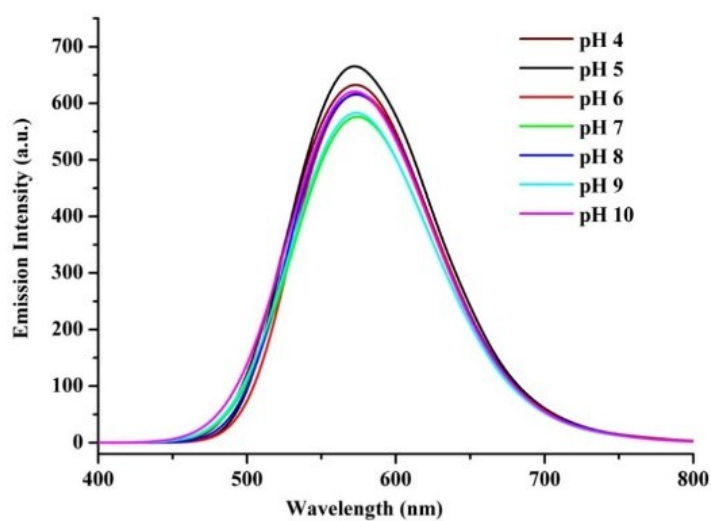


Figure S23. Phosphorescence spectra of **2d** in various pH buffer solutions (the phosphorescent emissions remained unchanged within a wide pH range of 4–10).

Photostability: Photostability of **2d**, and Mito-Tracker-Red was monitored by the absorption intensity in ethanol (1×10^{-5} M) under irradiation. The solution in a 1 cm square quartz cuvette was irradiated using a 300 W Xe lamp (Asahi spectra, MAX-302) equipped with a 325 nm cutoff filter.

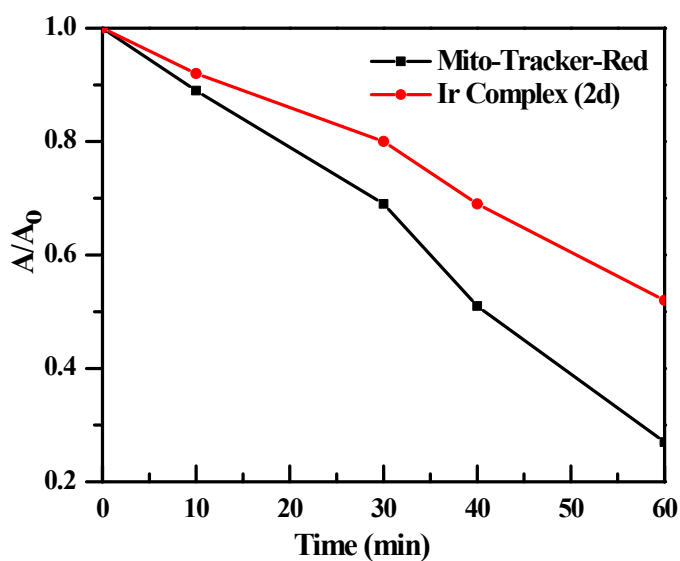


Figure S24. Photostability comparison of **2d** with Mito-Tracker-Red. All data are presented as mean \pm standard deviation ($n = 3$) (indicating complex **2d** is photostable)

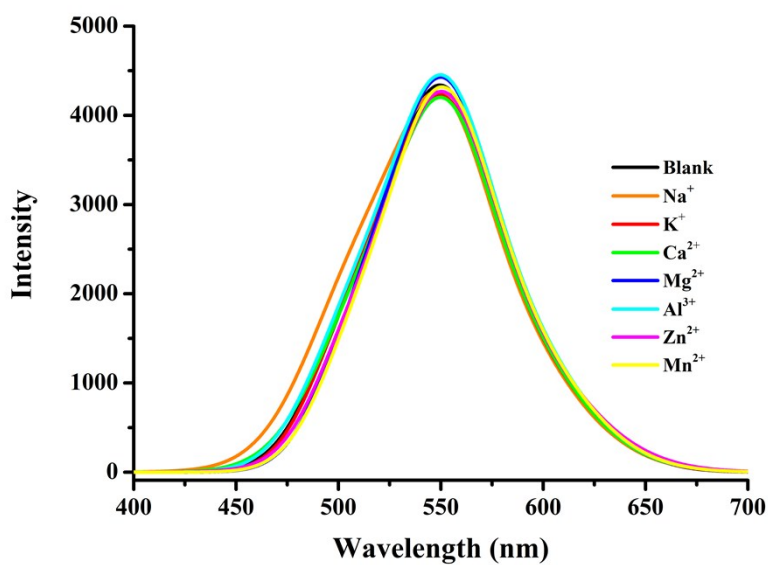


Figure S25. Phosphorescence spectra of **2d** (1×10^{-5} M) in the presence of various metal ions (Na^+ , K^+ : 5 mM; Ca^{2+} , Mg^{2+} : 500 μM ; Zn^{2+} , Al^{3+} , Mn^{2+} : 200 μM). The phosphorescent emission intensity remained almost unchanged and the common metal ions have very little effect on the phosphorescent emission intensity.

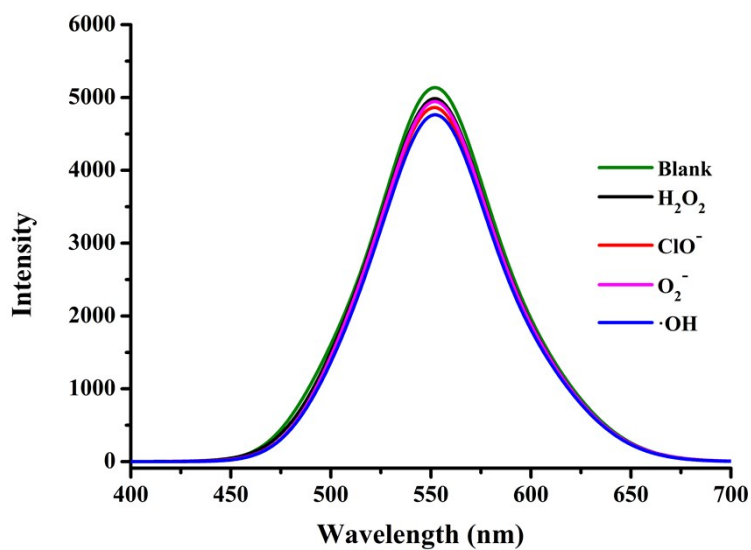


Figure S26. Phosphorescence spectra of **2d** (1×10^{-5} M) in the presence of various ROS (H_2O_2 : 50 μM ; other ROS: 100 μM). All the ROS species have very little effect on the phosphorescent emission intensity.

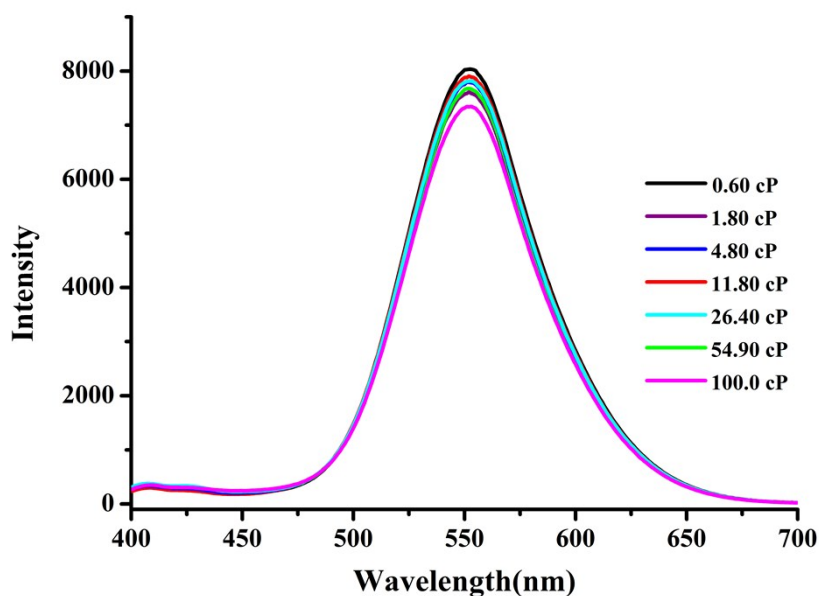


Figure S27. Phosphorescence emission spectra of **2d** (1×10^{-5} M) in methanol-glycerol solvent system with different proportions (methanol, $\eta = 0.60$ cP; glycerol, $\eta = 945.35$ cP). The emission intensity changes very little with increasing the viscosity from 0.60 cP to about 100 cP.

To evaluate the cytotoxicity of **2d** in living cells, in vitro test was measured using a standard methyl thiazolyl tetrazolium (MTT, Sigma Aldrich) assay with HepG2 celllines. Briefly, cells growing in log phase were seeded into 96–well cell culture plate at 1×10^4 / well. Complex **2d** was added to wells of the treatment group at concentrations of 5, 10, 50, 75 and 100 $\mu\text{mol/L}$. For the negative control group, 1 μL /well solvent was diluted in RPMI 1640 to the final concentration of 1%. The cells were incubated for 48 h at 37 $^\circ\text{C}$ under 5% CO_2 . Combined MTT/PBS solution was added to each well of the 96–well assay plate and incubated for another 4 h. After removal of the culture solution, 200 μL DMSO was added to each well, shaking for 10 min at a shaking table. An enzyme–linked immunosorbent assay (ELISA) reader was used to measure the OD570 (absorbance value) of each well referenced at 490 nm. The following formula was used to calculate the viability of cell growth: Viability (%) = (mean of absorbance value of treatment group / mean of absorbance value of control) $\times 100$.

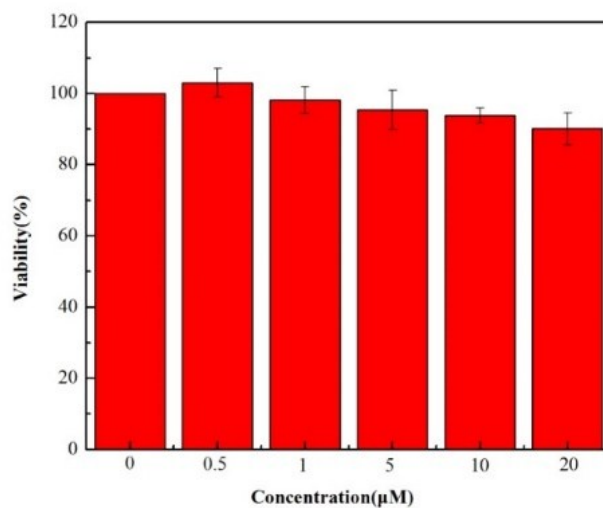


Figure S28: In vitro cell viability of HepG2 cells incubated with complex **2d** at different concentrations for 48 h.

VII. Confocal luminescence imaging and phosphorescence lifetime

imaging: Confocal luminescence imaging was carried out on an Olympus IX81 laser scanning confocal microscope equipped with a 40 immersion objective lens. A semiconductor laser was served as excitation at 405 nm of the HepG2 cancer cells pre-incubated with complex **2d**. The one-photon emission was collected at 450–550 nm range for model complex in HepG2 cancer cells. Complex **2d** was added to yield 10 μM solution and the HepG2 liver cancer cells were incubated with the solution of complex **2d** for 1 hour at 37 °C for live-cell imaging. The incubation of 10 μM complex **2d** and Annexin–FITC in the dead HepG2 cells, which were later fixed by addition of 4% paraformaldehyde / 2.5% glutaraldehyde for 1 h, was subject to the dead-cell imaging. In the case of apoptosis imaging experiments, HepG2 cells were grown on coverslips (Fisher Scientific, Atlanta, GA) in DMEM. To induce apoptosis, HepG2 cells were then incubated with Apoptosis Inducers Kit for up to 10 h. Afterwards, the cells were washed with PBS and incubated for 10 min at 37 °C with 10 μM complex **2d** and Annexin V–FITC. Finally, the cells were fixed onto coverslips with 2 wt% formaldehyde. PLIM image setup is integrated with Olympus IX81 laser scanning confocal microscope. Phosphorescence signal was detected by confocal microscope, and correlative calculation of the data was performed by professional software which was provided by PicoQuant Company. Light from the pulse diode laser head (PicoQuant, PDL 800–D) with excitation wavelength of 405 nm and frequency of 0.5 MHz was focused on the sample with a 40x/NA 0.95 objective lens for single-photon excitation. The emitted phosphorescence signal was collected at 550–650 nm for complex **2d** in cancer cells.

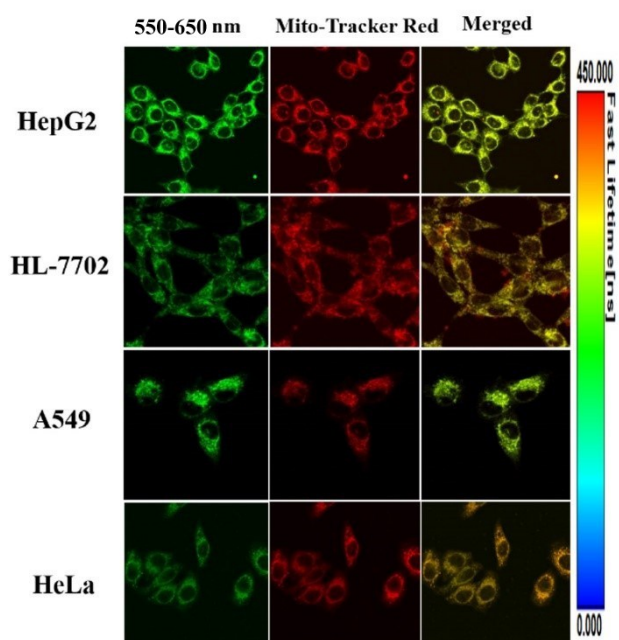


Figure S29. The co-localization phosphorescence images of complex **2d** in different cells

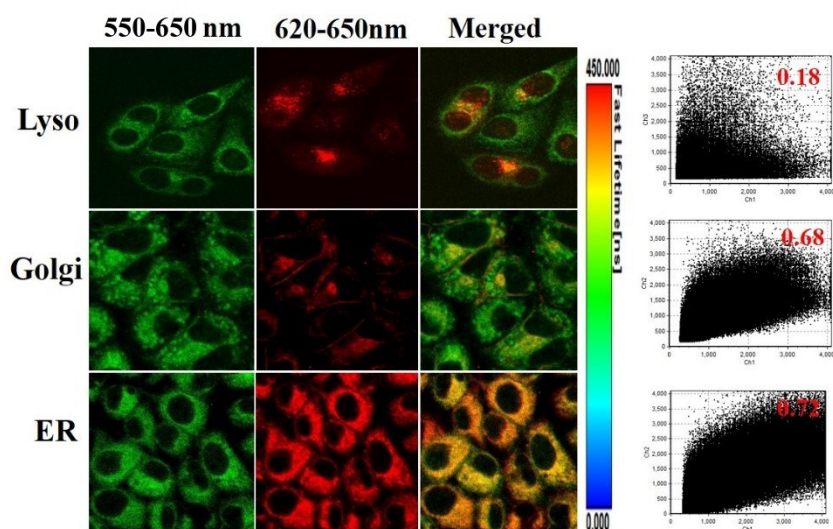


Figure S30. The co-localization phosphorescence images of complex **2d** in different organelles in HepG2 cells stained at 10 μ M concentration (these experiments indicate that complex **2d** can preferentially accumulate in mitochondria).

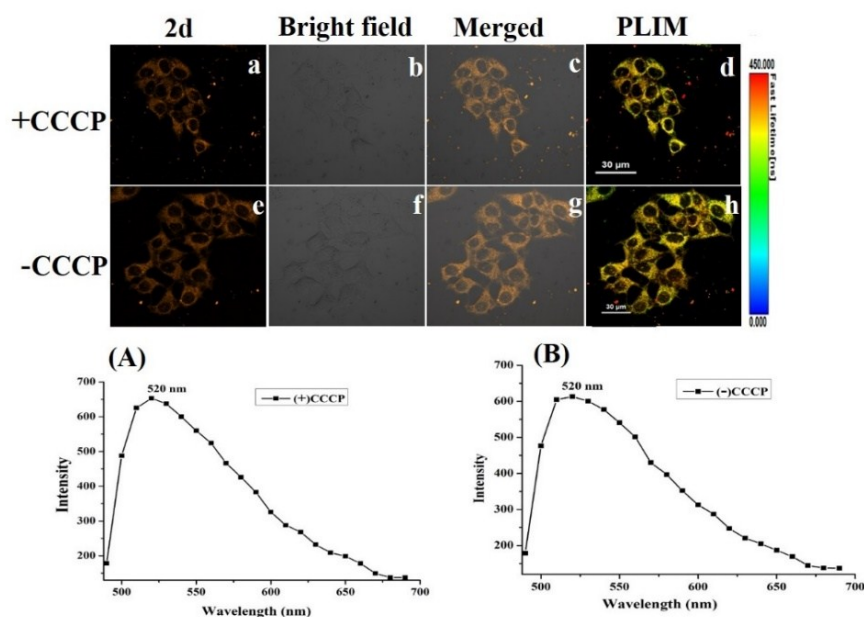


Figure S31. (Up) Confocal phosphorescence images of HepG2 cells stained with complex **2d** (0.1 μM, $\lambda_{\text{ex}} = 405$ nm) in the absence (e–h) or presence (a–d) of CCCP (10 μM). (Down) Emission spectra upon excitation ($\lambda_{\text{ex}} = 405$ nm) of complex **2d** within the cells (indicating that complex **2d** is independent of mitochondrial membrane potential).

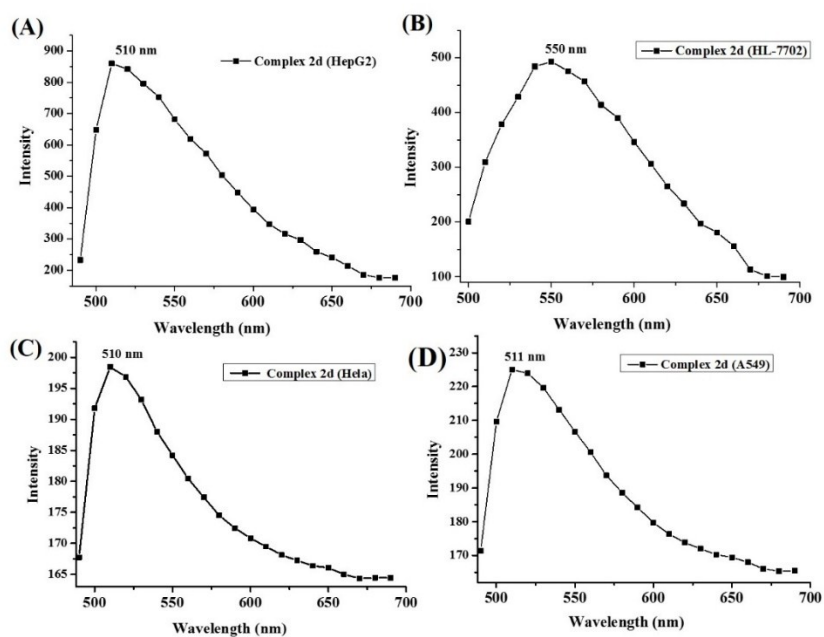


Figure S32. Emission spectra upon excitation ($\lambda_{\text{ex}} = 405$ nm) of complex **2d** in different cells (emission spectra within the cells were nearly identical to those observed for **2d** in the extracellular environment).

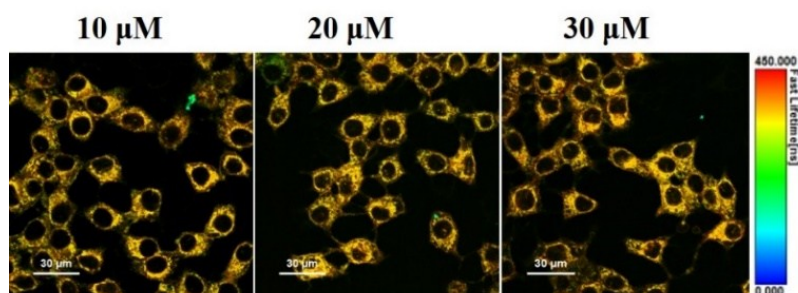
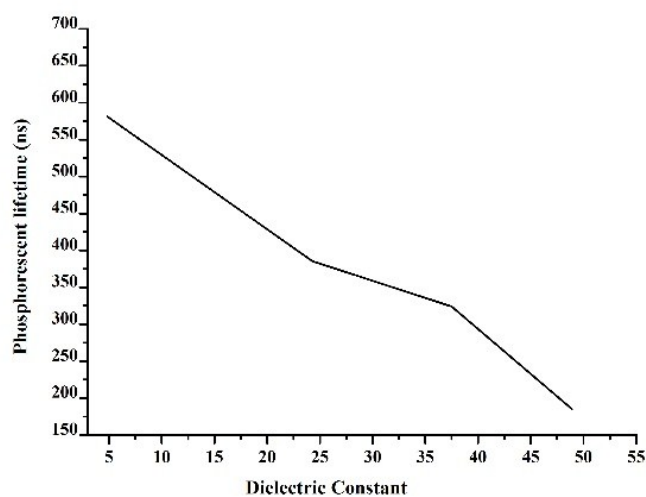


Figure S33. Phosphorescent lifetime imaging in HepG2 cells stained with complex **2d** at different concentrations. (10, 20, and 30 μM) (demonstrating that the probe is stable during the measurement of imaging).



	Toluene	DCM	CHCl_3	EtOH	CH_3CN	DMSO
λ_{ex} = nm	535	563	553	567	574	577
τ (ns)	794.5	760	581.5	385.5	324.1	185.2
Quantum yield	0.80	0.79	0.72	0.40	0.34	0.21

Figure S34. The lifetime of complex **2d** exhibits as a function of solvent polarity.

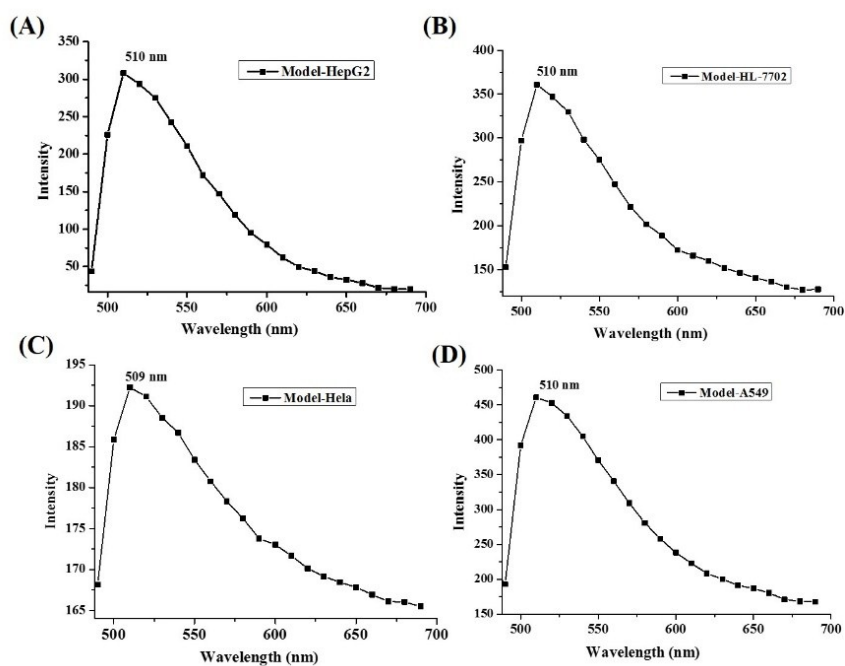
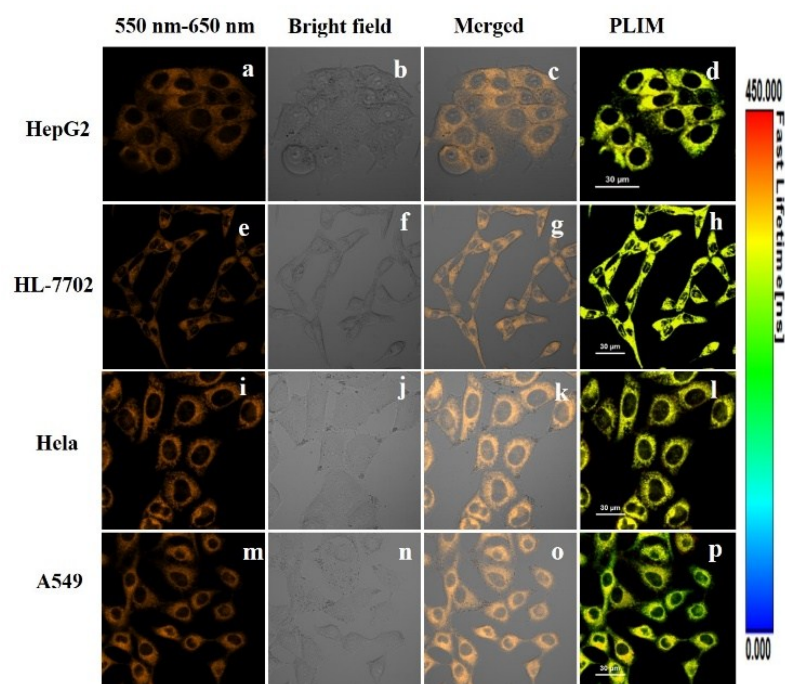


Figure S35. (Up) Phosphorescent lifetime imaging in HepG2, HL-7702, Hela, and A549 cells stained with **Model** complex (10 μ M); (Down) Emission spectra upon excitation ($\lambda_{\text{ex}} = 405 \text{ nm}$) of **Model** within cells (emission spectra within the cells were nearly identical to those observed for **Model** in the extracellular environment).

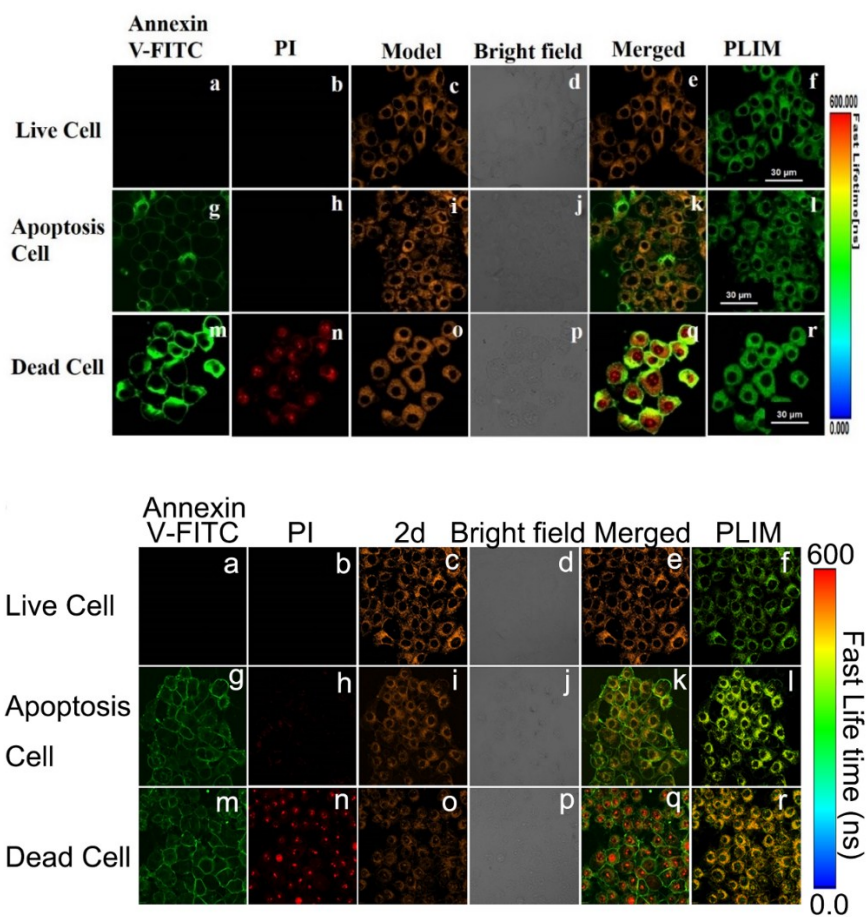


Figure S36. Phosphorescent lifetime imaging of HepG2 cells in different states stained with **Model** complex (10 μ M, up) and **2d** (10 μ M, down).

VIII. References

- [S1]: a) S. Lamansky, P. Djurovich, D. Murphy, F. Abdel-Razzaq, H. E. Lee, C. Adachi, P. E. Burrows, S. R. Forrest and M. E. Thompson, *J. Am. Chem. Soc.* **2001**, *123*, 4304–4312.
- [S2]: a) M. D. Marshall, R. M. Hunt, G. T. Hefferan, R. M. Adams and J. M. Makhlouf, *J. Am. Chem. Soc.* **1967**, *89*, 3361–3362. b) J. M. Makhlouf, W. V. Hough and G. T. Hefferan, *Inorg. Chem.* **1967**, *6*, 1196–1198. c) I. B. Sivaev, A. V. Prikaznov and D. Naoufal, *Collection. of Czechoslovak. Chem. Commun.* **2010**, *75*, 1149–1199. c) R. N. Grimes, *Carboranes*; 2nd ed., Vol. 9, Academic Press: New York, 2011, pp. 301–540. d) D. Power and T. R. Spalding, *Polyhedron* **1985**, *4*, 1329–1331. e) A. Toppino, A. R. Genady, M. E. El-Zaria, J. Reeve, F. Mostofian, J. Kent and J. F. Valliant, *Inorg. Chem.* **2013**, *52*, 8743–8749. f) L. A. Galliamova, M. V. Varaksin, O. N. Chupakhin, P. A. Slepukhin and V. N. Charushin, *Organometallics* **2015**, *34*, 5285–5290.
- [S3]: a) X. Li, X. Tong, H. Yan, C. S. Lu, Q. Zhao, W. Huang, *Chem. Eur. J.* **2016**, DOI: 10.1002/chem.201603440. b) C. Baik, Z. M. Hudson, H. Amarne, S. N. Wang, *J. Am. Chem. Soc.* **2009**, *131*, 14549–14559. c) Y. Yasu, T. Koike, M. Akita, *Chem. Commun.* **2013**, *49*, 2037–2039.
- [S4]: M. J. Frisch, G. W. Trucks, H. B. Schlegel, G. E. Scuseria, M. A. Robb, J. R. Cheeseman, G. Scalmani, V. Barone, B. Mennucci, G. A. Petersson, H. Nakatsuji, M. Caricato, X. Li, H. P. Hratchian, A. F. Izmaylov, J. Bloino, G. Zheng, J. L. Sonnenberg, M. Hada, M. Ehara, K. Toyota, R. Fukuda, J. Hasegawa, M. Ishida, T. Nakajima, Y. Honda, O. Kitao, H. Nakai, T. Vreven, J. A. Montgomery Jr., J. E. Peralta, F. Ogliaro, M. Bearpark, J. J. Heyd, E. Brothers, K. N. Kudin, V. N. Staroverov, T. Keith, R. Kobayashi, J. Normand, K. Raghavachari, A. Rendell, J. C. Burant, S. S. Iyengar, J. Tomasi, M. Cossi, N. Rega, J. M. Millam, M. Klene, J. E. Knox, J. B. Cross, V. Bakken, C. Adamo, J. Jaramillo, R. Gomperts, R. E. Stratmann, O. Yazyev, A. J. Austin, R. Cammi, C. Pomelli, J. W. Ochterski, R. L. Martin, K. Morokuma, V. G. Zakrzewski, G. A. Voth, P. Salvador, J. J. Dannenberg, S. Dapprich, A. D. Daniels, O. Farkas, J. B. Foresman, J. V. Ortiz, J. Cioslowski, D. J. Fox, Gaussian 09, Revision B.01, Gaussian, Inc., Wallingford CT, 2010.